NOTE TO USERS

Multipath Detection in CDMA Systems

Mohamed A. Abou-Khousa

A Thesis

in

The Department

of

Electrical and Computer Engineering

Presented in Partial Fulfillment of the Requirements

for the Degree of Master of Applied Science in Electrical Engineering

Concordia University

Montreal, Quebec, Canada

January 2005

Your file Votre référence
ISBN: 0-494-04359-8
Our file Notre référence
ISBN: 0-494-04359-8

Abstract

Multipath Detection in CDMA Systems

Mohamed A. Abou-Khousa

This thesis addresses the problem of multipath detection in CDMA systems. In conventional CDMA receivers, the detection of multipath components and RAKE finger management is normally based on the received signal energy per path. These energy-based schemes essentially overlook the interference component contaminating the total received power. Consequently, they exhibit poor detection capability especially at low signal-to-interference-plus-noise ratio (SINR). In this thesis, we present a new scheme for multipath detection and RAKE finger assignment that takes into consideration the interference level in each resolved path individually. The proposed scheme utilizes information provided by the pseudo random code acquisition circuit to estimate the interference power per path. To account for the hardware limitations of the receiver, a low complexity version of the proposed scheme is designed and incorporated into the receiver structure Analytical and simulation results show that the proposed scheme provides significant improvements in the detection probability of multipath components over the energy-based schemes. For instance, our results show that the proposed scheme can achieve the same detection probability of all multipath

components as that of the energy-based scheme with a saving of at least 2 dB in E_b/N_0. In some cases, it is shown that the improvement can be as high as 3 dB.

To Abd-allah's daughter; the greatest mother of a kind, my father, sisters, and brothers...

Acknowledgments

First and foremost thanks to ALLAH for all that I am and all that I have accomplished. Thereafter, the most elegant gratitude is always pertained to my parents, brothers, and sisters to whom I am dedicated. I would like to convey my sincere appreciation to my supervisors; Dr. Ali Ghrayeb and Dr. Mohamed El-Tarhuni, who guided me through this endeavor with endless support, encouragement, and patience.

Many special thanks are also related to Dr. N. Qaddomui and Mr. W. Saleh for their continuous trust.

It is also my delight to thank Mr. M. H. Moussa, Ms. Xiangnian Zeng, and my other colleagues in Dr. Ghrayeb's research group for their valuable comments and help.

Contents

List of Figures

List of Tables

Chapter 1

Introduction

Over the past two decades, we have witnessed a drastic increase in the demand for providing reliable wireless communication links to support high-speed data transmission applications. Such applications include voice, video, e-mail, web browsing, etc. This demand has been the driving force behind the migration from the second generation (2G) system to the third generation (3G) system. The 3G services, which have been standardized around the world, are mainly based on the code division multiple access (CDMA) technology. Prominent examples of existing systems that employ CDMA are the cdma2000 and wideband-CDMA (WCDMA) systems.

In 3G CDMA systems, the signals transmitted are wideband in nature, which gives rise to *multipath propagation.* Although multipath fading may seem harmful because different replicas of the same signal may add destructively at the receiver, it

can be exploited at the receiver to improve the performance relative to the case when there is no multipath. A key issue for dealing with multipath fading is to first identify the potential paths at the front end of the receiver. Then, a RAKE receiver is used to coherently combine the energy from these multipath components, and hence the exploitation of inherent frequency diversity in the channel.

A RAKE receiver basically consists of several correlators called *fingers* that are time-aligned with the different paths. Each finger is intended to de-spread the corresponding path and then the outputs of these fingers are properly combined to maximize the signal-to-interference-plus-noise ratio (SINR) at the output of the RAKE receiver. As such, the RAKE receiver can be thought of as a matched filter that is matched to the channel impulse response.

Matching the RAKE to the channel impulse response essentially requires the receiver's knowledge of the potential multipath components in the channel and the channel fading coefficients of these components. During traffic mode, the receiver dynamically searches for candidate multipath components for combining. Once these paths are detected, they are fine aligned (brought within a fraction of a chip from each other) with respect to the locally generated user's spreading code, and then assigned to the RAKE fingers. The channel fading coefficients are estimated for the assigned paths and used in the RAKE for coherent combining, i.e., maximum ratio combing (MRC) of the assigned paths.

Clearly, missing potential paths or assigning incorrect paths to the RAKE fingers will result is a loss in the diversity order achieved, as well as in an increase in the

interference level after combining. In such cases, the overall system performance will deteriorate significantly. In light of this, the criterion by which the multipath components are detected and assigned to the RAKE fingers should be devised such that the probability of detecting the correct paths is maximized and the probability of combining the incorrect paths is minimized [1] [2].

In conventional CDMA receivers, the multipath components are detected using a search block and an acquisition circuit [3] [4]. The search block correlates the received signal with locally generated shifted versions of the intended user's pseudo random (PN) code, and the correlation results are then presented to an acquisition circuit. In the acquisition circuit, the correlation results are subjected to hypotheses testing using a pre-calculated threshold [1]−[5]. The resolvable paths with energy exceeding this threshold are detected and assigned to the available RAKE fingers for combining. In case the number of these paths is greater than the number of available fingers, the paths with maximum energy among the potential paths are selected and combined [2], [6]−[8]. The process by which these paths are detected and assigned to the RAKE fingers is commonly referred to as the *finger assignment algorithm* (FAA).

Normally, deciding on what paths to combine at the RAKE receiver depends on several factors, including the available number of fingers, energy content per path, and the inter-path separation. For instance, if the number of available fingers is greater than the number of resolvable paths, it may not be a good idea to combine weak paths since they will contribute more noise to the combiner output and hence may degrade the bit-error-rate (BER) performance of the system. In this case, however,

it may be useful to combine strong paths that are within a fraction of a chip apart, i.e., correlated paths, if extra fingers are available at the receiver [7].

Conventionally, the paths with maximum 'total' energy are detected and assigned to the available RAKE fingers. This scheme is referred to here as energy-based multipath detection scheme (EMDS). There are two FAA strategies available in the literature for assigning RAKE fingers to detected multipath components based on the EMDS [6]. The first strategy assigns the paths with the largest instantaneous amplitudes to the available fingers. This strategy is well suited for cases when the channel coefficients are slowly changing during the search process for new paths. The second strategy assigns the paths with the largest average powers to the available fingers, which is applicable when the fade rate is comparable to or larger than the search rate.

Although the conventional multipath detection and finger assignment schemes are deemed to be practical from an implementation point of view, they suffer from major drawbacks. Mainly, the correlation energy, based on which the multipath components are detected, is typically comprised of the desired signal energy and the interference coming from other multipath components belonging to the desired user as well as other users. At low SINR, the desired user's multipath components are vulnerable to be 'masked' by other paths with large interference power. Consequently, the probability of detection deteriorates considerably.

Additionally, the conventional multipath detection scheme does not maintain a constant false alarm rate (CFAR). This is an undesirable phenomenon which may become significant particularly in multi-access fading channels where the desired user's

signal as well as the interference level fluctuate with time. In an effort to address this issue, many researchers have recently proposed adaptive acquisition schemes (AAS) which involve using an adaptive threshold to encompass the changes in the interference level [9]−[14]. However, it was shown in [9] that the performance of these schemes is highly affected by the presence of multipath components in the search window. To reduce the effect of the multipath propagation on the AAS performance, a detection scheme based on removing the multipath components from the search window before estimating the interference level was proposed in [11] and [12]. Although this scheme has theoretically reported promising results, its major drawback is that the multipath components to be removed should be identified first.

In [13], an adaptive PN acquisition scheme based on estimating the interference power using a moving average filter over the search results was proposed. In deriving the probability of detection and probability of false alarm for this scheme, the estimation of the interference power was considered to be perfect assuming that the filter length is large enough. However, this assumption becomes practically invalid when the channel changes rapidly. Furthermore, the design of the moving average filter was not addressed rigorously in [13].

In the conventional energy based FAA, the finger assignment is based upon the assumption that the multipath interference at all fingers are mutually uncorrelated and have equal energy. However, this is not always the case. For instance, if we consider the forward link in CDMA systems, the multipath interferences may differ

in energy magnitude from one finger to another as illustrated in [15] and [16]. Therefore, finger combining based on signal strength alone does not achieve maximal-ratio combining [17]. Consequently, a better combining strategy should consider combining the paths with maximum SINR rather than the ones with maximum total energy contents [18]−[20]

In the advanced spreading techniques, the performance of the recently proposed space-time spreading (STS) scheme is highly affected by delay and channel estimation errors. Hence, there is an increasing demand for detection schemes that are more efficient than the conventional EMDS. In particular, a detection scheme that exhibits more immunity against the co-channel interference is sought.

In this work, we investigate and analyze the performance of the conventional energy-based multipath detection scheme (EMDS). It will be shown that the major drawback of the EMDS is that its decision metric depends on both the power of the desired user as well as that of the interference. Consequently, the probability of detection becomes directly proportional to the interference power. To overcome the above deficiency, we propose an improved multipath detection scheme (IMDS) that addresses the problems of the conventional scheme. The efficacy of the proposed scheme stems from its capability of estimating the interference level at each delay offset in the search window using a practical estimator at the *acquisition stage*. This feature of the proposed scheme allows for taking the interference component into consideration more effectively in the multipath detection process.

As compared to the AASs presented in the literature, the proposed detection

scheme does not suffer from any performance degradation due to the existence of multipath components in the search window. This is especially true since the IMDS is based on estimating the interference variance per delay offset in the search window, thereupon, subtracting these estimates from the total signal power before the detection decision is made. This is basically different from the approach behind the existing AASs which rely on averaging the search results over the delay offsets other than the one under examination. As it has been shown in [9], when multipath components exist in the search window, averaging around a certain delay within the search window does not provide accurate estimate of the interference.

We also address the problem of multipath detection in STS-based CDMA systems. We extend both the conventional EMDS and the IMDS to cope with the spatial channel structure. By simulations, we investigate the effect of imperfect multipath detection resulting from both the EMDS and IMDS on the performance of the STS scheme.

This thesis is aimed to meet the following objectives.

- To evaluate the performance of the EMDS in a realistic communication environment.
- To improve upon the EMDS by introducing a cost effective detection scheme.
- To study the performance of the STS-based CDMA systems with imperfect multipath detection.

The intellectual contributions presented in this work are summed up in the following points.

1. This thesis offers an in-depth analysis and comprehensive performance evaluation of the conventional energy based multipath detection scheme for CDMA systems operating over frequency selective fading channels. Expressions for the probability of detection and probability of false are derived when many multipath components are present in the search window.

2. An improved multipath detection scheme is developed, analyzed, and compared to the conventional scheme under various operational conditions. The probability of detection and probability of false for the proposed scheme are derived. A low complexity version of the proposed scheme is also introduced and incorporated into the receiver structure. To furnish the low complexity realization of the proposed scheme, a customized design procedure is developed and implemented.

3. The impact of multipath detection on the performance of the STS-based CDMA systems is investigated using both the conventional and the improved multipath detection schemes. Both detection schemes are extended to work on the signal model assumed by the STS scheme. The performance of the conventional scheme is compared to that of the proposed scheme.

The remaining parts of this thesis are organized as follows. In Chapter 2, the problem of multipath detection in the CDMA systems is tackled. Chapter 3 is devoted

to investigate the impact of multipath detection on the performance of the of the CDMA systems with space-time spreading. Finally, the conclusions drawn from this thesis and the suggested future work are presented in Chapter 4.

Chapter 2

Improved Multipath Detection for CDMA Systems

In this chapter, we investigate and analyze the performance of the conventional energy-based multipath detection scheme (EMDS). We propose an improved multipath detection scheme (IMDS) that addresses the problems of the conventional scheme. The efficacy of the proposed scheme stems from its capability of estimating the interference level at each delay offset in the search window using a practical estimator at the acquisition stage. This feature of the proposed scheme allows for taking the interference component into consideration more effectively in the multipath detection process.

In Section 2.1, we describe the adopted system model and the receiver search mechanism for multipath components. Detailed analysis and description of the energy-based multipath detection scheme (EMDS) are given in Section 2.2. We derive the

probability of detection and the probability of false alarm for the EMDS. Thereafter, the energy-based finger assignment algorithm is outlined.

Before developing the improved multipath detection scheme, the estimators that will be used to realize this scheme are pinned down in Section 2.3. The per path interference variance estimator is developed when the channel coefficients are perfectly known. We also derive the Cramer-Rao bound (CRB) for that estimator. Then, an optimum channel estimator derived based on the knowledge of the channel autocorrelation function is presented. The structure of this estimator will be used later as a design benchmark to realize a low complexity improved multipath detection scheme.

Section 2.4 is devoted for the improved multipath detection scheme (IMDS) which will be developed based on the per path interference variance estimator presented in Section 2.3. The probability of false alarm and probability of detection of the IMDS will be derived. Furthermore, a practical realization of IMDS will be designed by the aid of the optimum channel estimator introduced in Section 2.3.

In Section 2.5, the performance of the IMDS and the EMDS will be evaluated and analyzed by computer simulations. Finally, Section 2.6 concludes this chapter.

2.1 System Model

The system considered in this work is similar to that of the reverse link of the proposed third generation cdma2000 system where a pilot channel is code multiplexed with the data channel. The pilot channel is used for code synchronization (acquisition and

tracking), channel estimation, and signal strength measurement. More specifically, we consider a direct-sequence spread-spectrum (DS-SS) system where the base-band BPSK transmitted signal from the desired user is modeled as

$$s_1(t) = \sum_i \sum_{j=0}^{N_c-1} \left(\sqrt{E_{b1}} d_{1i} W_j + \sqrt{G_p} \right) c_{1j} g(t - iT_b - jT_c) \tag{2.1}$$

where $\sqrt{E_{b1}}$ is the average bit energy, $d_{1i} \in \{\pm 1\}$ is the i^{th} information bit, $W_j \in \{\pm 1\}$ is a Walsh code used to separate the pilot channel from the traffic channel, G_p is the pilot channel power gain relative to the traffic channel (typically -3 dB or $0.5E_b$), $c_{1j} \in \{\pm 1\}$ is the spreading pseudorandom (PN) code of the desired user, N_c is the PN code spreading factor which is the same as the number of chips per bit, $g(t)$ is the chip pulse shape, T_b is the bit duration, and T_c is the chip duration. The DS-SS signal given by (2.1) is constructed using the circuit depicted in Figure 2.1. The pilot symbols are assumed to be all ones[1].

The transmitted signal passes through a mobile radio channel with L time varying paths. In a wide sense stationary uncorrelated scattering (WSSUS) environment, these paths are represented by the channel coefficients $\{\alpha_l : l = 1, 2, \ldots, L\}$, where these coefficients are modeled as independent and identically distributed (i.i.d.) complex Gaussian random variables with zero mean and variance 0.5 per dimension, i.e., $|\alpha_l|$ is Rayleigh distributed and the phase is uniformly distributed in $[0, 2\pi)$. The channel coefficients are assumed to be constant during a symbol duration, i.e., N_c

[1]We remark that the system model presented here is a simplified version of the one adopted by cdma2000 standard. For a complete description of the cdma2000 standard, the interested reader may see [34].

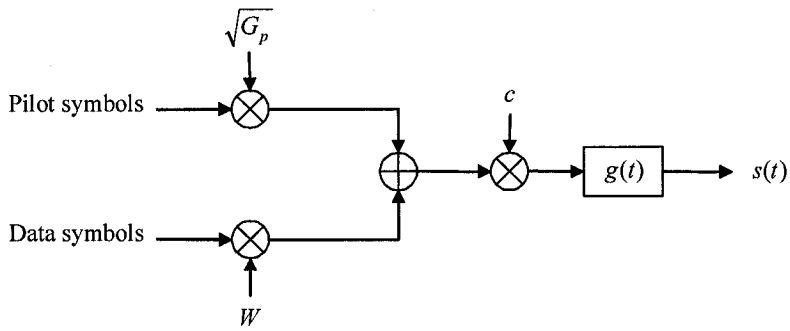

Figure 2.1: BPSK spreading circuit with the pilot symbols are code-multiplexed with the data.

chips. Furthermore, the in-phase and quadrature components of any channel coefficient are assumed to be independent from each other [21]. In general, the average power at the output of the channel as a function of the time delay, i.e., the channel power delay profile (PDP), is denoted by $\phi(l)$.

The received baseband signal at the base station receiver is then given by

$$u(t) = \sum_{m=1}^{M} \sum_{l=1}^{L} \sqrt{\phi(l)} \alpha_{ml} s_m(t - \tau_{ml}) + n(t) \tag{2.2}$$

where α_{ml} and τ_{ml} are the channel gain and path delay for the l^{th} path of the m^{th} user, respectively, and $n(t)$ is a complex additive white Gaussian noise (AWGN) process with zero mean and power spectral density $N_0/2$ per dimension. Throughout this investigation, perfect power control is assumed, i.e., the interfering users in the system impinge at the base station receiver with equal power.

2.1.1 CDMA Receiver Structure

The block diagram depicted in Figure 2.2 shows the structure of the CDMA receiver considered in this investigation. The received signal is first applied to a multipath search block (henceforth referred to as *searcher*). The searcher looks for potential multipath components in the desired user's channel. The search results are then presented to multipath detection logic. According to this logic, the potential multipath components are selected, fine aligned by a Delay Lock Loop (DLL), and yet further processed by the finger assignment algorithm before they are allocated to the RAKE fingers. The fading channel coefficients are estimated for the assigned paths and used for coherent combining in the RAKE. The channel is typically estimated using a moving average filter after despreading the pilot symbols as described in [22].

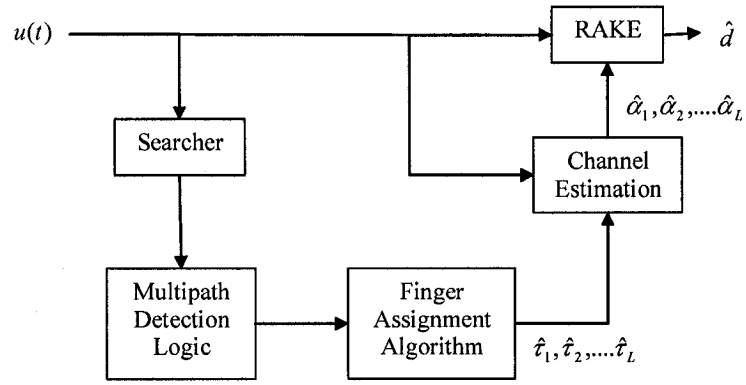

Figure 2.2: The assumed CDMA receiver structure.

In this work, we are mainly interested in the multipath detection logic and the finger assignment algorithm. We will start by presenting the multipath search procedure before we describe the schemes used for multipath detection.

2.1.2 The Searcher

The 3G CDMA systems have wide transmission bandwidth and are intended to support high data rates over the wireless channels. The intrinsic bandwidth expansion of the transmitted signal upholds an increase in the time dispersion of the channel. Consequently, the receiver experiences an increased multipath resolution. In the wireless channel and due to the movement of the mobile terminal, the delays as well as the amplitudes of the resolvable paths are non-stationary, hence it becomes essential for the receiver to search dynamically for new multipath components in the channel. In the case if an already-assigned delay disappears, that delay is de-assigned, and new 'stronger' path will be assigned to the vacant finger [7]. The interworking mechanism between detection, assignment and tracking processes is shown in Figure 2.3.

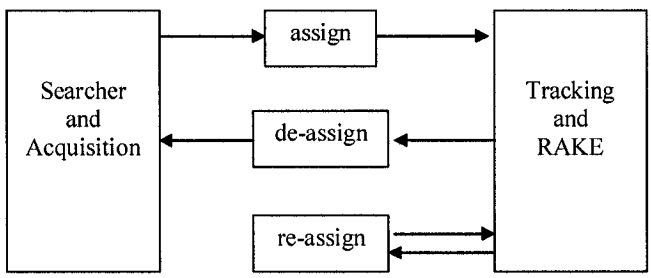

Figure 2.3: The functional interworking between delay detection, assignment, and tracking.

During the data traffic transmission (traffic mode), the receiver searches continuously for new potential multipath components to be combined in the de-modulation stage. The search algorithm is basically an integral part of the acquisition circuit used to perform the correlation between the received signal and different replicas of

the desired user's PN code. Basically the searcher *despread* the incoming signal using different time shifted versions of the user's code.

The searcher examines a window of C possible delays for a period of time (dwell time T_d), and the correlation results are stored for further processing. The search step size, denoted by S, is typically a fraction of a chip, e.g., one-half a chip. The delay uncertainty region consists of $K = C/S$ delay offsets. The time span of the uncertainty region is normally set according to the *Channel Excess Delay*, defined as the length of the channel impulse response for a power exceeding a given power threshold [7]. Thus, the channel excess delay defines the delay search window to be examined by the searcher.

Without loss of generality, T_d is assumed equal to the bit duration T_b. Hence, the search results, which we call the *search delay profile*, will consist of $K = C/S$ values where each value is given by

$$h_k(n) = f_{1k}(n) + f_{Ik}(n) + N_{kn} \tag{2.3}$$

where the index k represents the k^{th} delay offset within the search window and n is the search time index within received frame, $f_{1k}(n)$ is the contribution of the desired user's signal, $f_{Ik}(n)$ the interference component, and N_{kn} is the contribution of the AWGN noise. The searcher circuit used to produce the channel delay profile is shown in Figure 2.4.

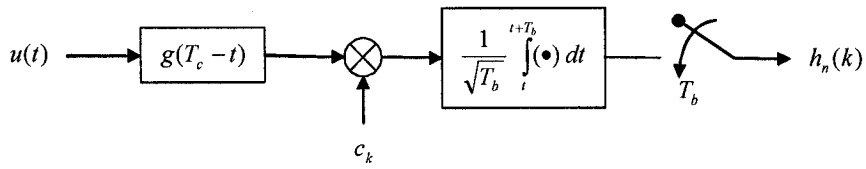

Figure 2.4: The signal detector used by the searcher.

The first two components of (2.3) can be shown to be

$$f_{1k}(n) = \sum_{l=1}^{L_1} \sqrt{\phi(l)}\alpha_{1l}(n)\left[\sqrt{E_{b1}}A_{11}(l,k)d_{1n} + \sqrt{G_p}B_{11}(l,k)\right] \tag{2.4}$$

and

$$f_{Ik}(n) = \sum_{m=2}^{M}\sum_{l=1}^{L_m} \sqrt{\phi(l)}\alpha_{ml}(n)\left[\sqrt{E_{bm}}A_{1m}(l,k)d_{mn} + \sqrt{G_p}B_{1m}(l,k)\right] \tag{2.5}$$

where E_{bm} and L_m are the m^{th} user average bit power and number of paths respectively,

$$A_{1m}(l,k) = \frac{1}{\sqrt{T_b}}\int_{T_b} W c_m c_1 g(t-\tau_l)g(t-\tau_k)dt, \tag{2.6}$$

and

$$B_{1m}(l,k) = \frac{1}{\sqrt{T_b}}\int_{T_b} c_m c_1 g(t-\tau_l)g(t-\tau_k)dt. \tag{2.7}$$

We remark that $A_{1m}(l,k)$ and $B_{1m}(l,k)$ scale the interference coming from the traffic

channel and the pilot channel, respectively, by the auto- and cross-correlation values of the shifted versions of the PN sequences assigned to different users.

The searcher should detect an effective path for the first user whenever l equals k, i.e., $\tau_l = \tau_k$, where the spreading code's autocorrelation function will be at its maximum. In this case, (2.4) can be re-written as

$$f_{1k}(n) = \sqrt{G_p \phi(k)}\alpha_{1k}(n) + \sum_{l \neq k}^{L_1} \sqrt{\phi(l)}\alpha_{1l}(n) \left[\sqrt{E_{b1}} A_{11}(l,k) d_{1n} + \sqrt{G_p} B_{11}(l,k)\right] \tag{2.8}$$

Substituting (2.8) into (2.3) yields

$$h_k(n) = \sqrt{G_p \phi(k)}\alpha_{1k}(n) + I_k(n) \tag{2.9}$$

where

$$I_k(n) = \sum_{l \neq k}^{L_1} \sqrt{\phi(l)}\alpha_{1l}(n) \left[\sqrt{E_{b1}} A_{11}(l,k) d_{1n} + \sqrt{G_p} B_{11}(l,k)\right] + f_{In}(k) + N_k. \tag{2.10}$$

The term $I_k(n)$ in (2.10) represents the total interference that is coming from other paths belonging to the desired user, interference from other users along with their multipath components, and the noise seen by the k^{th} delay offset. Under the standard Gaussian approximation, this term can approximated as AWGN [23]−[25]. This approximation is justified by the central limit theorem and holds when the number of the transmitting users in the system is large. With this assumption,

equation (2.9) is re-written as

$$h_k(n) = \sqrt{p(k)}\alpha_{1k}(n) + \sqrt{\sigma_I^2(k)}\bar{I}(n) \tag{2.11}$$

where $\bar{I}(n)$ is a normalized complex Gaussian random variable with zero mean and variance 0.5 per dimension, $p(k) = G_p\phi(k)$, and $\sigma_I^2(k)$ is the variance of the interference component.

To improve the probability of multipath detection, N_A independent search results are obtained through repeating the search process at different time instants, e.g. bits or search blocks, during a data frame. These time instants are usually chosen to be spaced sufficiently far from each other within a frame for the following reasons.

- To give the searcher the required time to correlate the received signal with all shifted versions of the PN code. In serial searcher circuits, the total time required is proportional to $K \times T_d$. This time is reduced considerably when a parallel searcher is utilized. This reduction comes at the expense of the increased complexity through implementing parallel correlators, especially if the search window is large [4] [5].

- To give the fading process some time to de-correlate. When the Doppler rate is high, the channel de-correlates faster, and hence the time spacing between the search results can be reduced and still the search results would be independent. The converse is true when the channel is slowly fading.

A schematic diagram showing the search blocks within a segment of the incoming

frame is depicted in Figure 2.5. The search blocks are used by the multipath detection scheme to measure the energy content of the examined delays. The searcher discards the blocks between the search blocks while processing the search results.

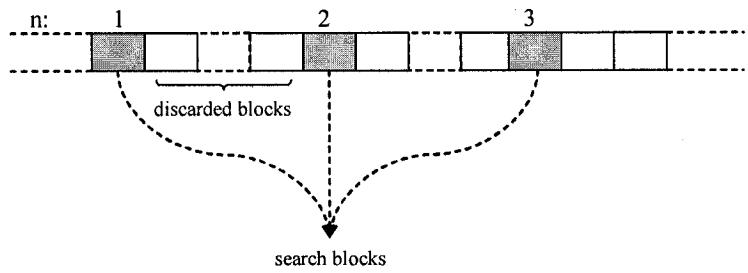

Figure 2.5: The search blocks within a segment of the incoming frame.

2.2 Energy-Based Multipath Detection Scheme (EMDS)

In the energy-based multipath detection schemes (EMDS), the correlation energies are averaged over N_A independent search blocks at each delay offset and the result is compared to a threshold. If the average energy at a certain delay offset exceeds the threshold, the path with that delay offset is acquired. This process is done for all delay offsets in the search window. The selected delay offsets are then fine-aligned through the tracking process, which is accomplished by employing a delay locked loop (DLL). If a wrong delay, which does not contain the desired user's signal, passes the threshold test, the tracking loop will detect it and declare a false alarm state after a relatively long period of processing time. Thus, it is extremely important to reduce the probability of false alarm of the detection scheme. The detection metric of the

EMDS is computed as shown in Figure 2.6.

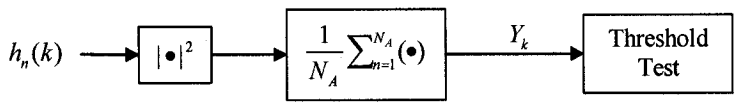

Figure 2.6: The EMDS detection metric computation.

From (2.11), the average correlation energy at the k^{th} delay offset is

$$\begin{aligned} Y(k) &= \frac{1}{N_A}\sum_{n=1}^{N_A}|h_k(n)|^2 \\ &= \tilde{p}(k) + \tilde{\sigma}_I^2(k) \end{aligned} \tag{2.12}$$

where $\tilde{\sigma}_I^2(k)$ is an estimate of the interference power $\sigma_I^2(k)$ obtained from N_A observations, and $\tilde{p}(k)$ is an estimate of the user power $p(k) = G_p\phi(k)$ obtained from N_A independent search samples. In (2.12), it is assumed that the interference and the desired user's signal are independent. This is a valid assumption since each multipath component fades independently as per the WSSUS model.

It can be shown that both variables $\tilde{\sigma}_I^2(k)$ and $\tilde{p}(k)$ have distributions that can be approximated by central Chi-square distributions with $2N_A$ degrees of freedom. The approximation holds well when the time-bandwidth product $N_A T_d/T_c$ is large [26].

The first and second order statistics of these variables are given as

$$\begin{aligned} E\{\tilde{\sigma}_I^2(k)\} &= \sigma_I^2(k), \\ var\{\tilde{\sigma}_I^2(k)\} &= \frac{\sigma_I^4(k)}{N_A}, \\ E\{\tilde{p}(k)\} &= p(k), \text{ and} \\ var\{\tilde{p}(k)\} &= \frac{p^2(k)}{N_A}. \end{aligned}$$

When $Y(k)$ exceeds the the threshold, then the k^{th} delay offset will be detected. Furthermore, if the RAKE receiver has L fingers, the k^{th}delay offset will be assigned to one finger if it is one of the L maximum components in the search window.

Apparently, when the SINR is low, some of the actual multipath components will be masked by other delay offsets with strong interference power, and consequently wrong paths will pass the threshold declaring a false alarm state.

To illustrate the concept behind the EMDS, consider the case when the desired user's channel contains 4 paths at relative delays 0, 2, 4, and 6 chips. Let us assume that the searcher examines a window of 16 chips looking for these delays. The decision metric given in (2.12) is computed from the search results at each delay offset. An example of the computed average energy profile (average energy per path) is shown in Figure 2.7 at signal-to-interference ratio $SIR = 10$ dB and average bit energy to noise power spectral density $E_b/N_0 = 20$ dB.[2] We remark that the values of the SIR and E_b/N_0 assumed here are quite unrealistic. However, they are used here to define

[2]While the SIR is defined before despreading, E_b/N_0 is defined at the output of the despreader.

a perfect detection event. As shown in the figure, since the average energy content of the paths at delays 0, 2, 4, and 6 chips exceed the threshold level at 0.1, these paths will be detected and assigned to the RAKE fingers (since they are the 4 maximums in the window). Furthermore, none of the other delays (other than the actual ones) has exceeded the threshold. Hence no false alarm has occurred

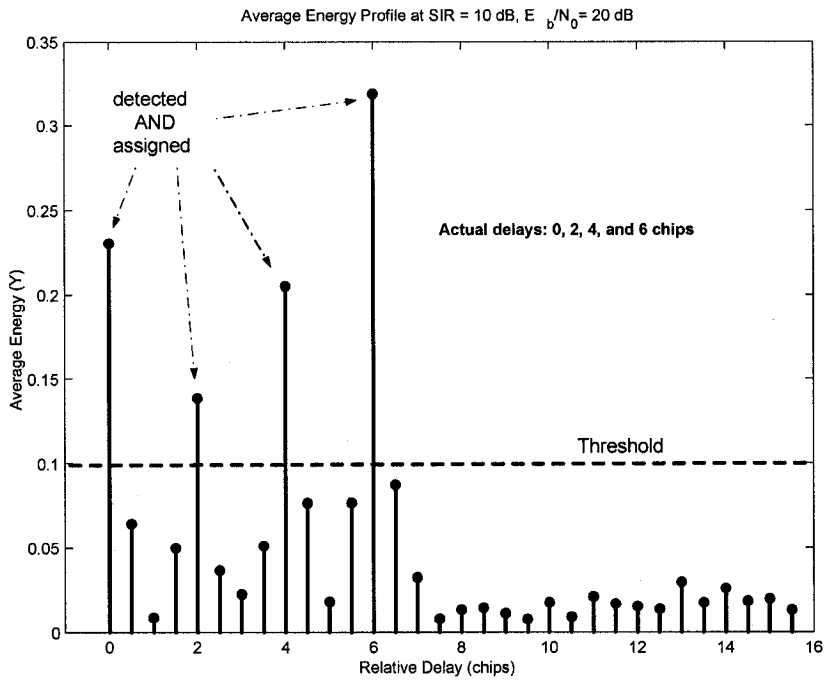

Figure 2.7: An illustrative example of the average energy profile at the examined delays with the EMDS.

Let us consider some practical figures for E_b/N_0 and SIR; say 7 dB and -10 dB respectively. The average energy profile is shown in Figure 2.8. As it is shown in the figure, some of the actual paths do have energy contents that exceed the threshold, and they are among the 4 maximums in the window, e.g. the paths at delays 4 and 6 chips. On the other hand, the *incorrect* paths at delays 10 and 11 chips are mistakenly

detected and assigned. This basically defines the false alarm event. Because of noise and interference the actual path at delay 0 chip is missed. Furthermore, the path at delay 2 chips is *masked* by other paths with stronger power.

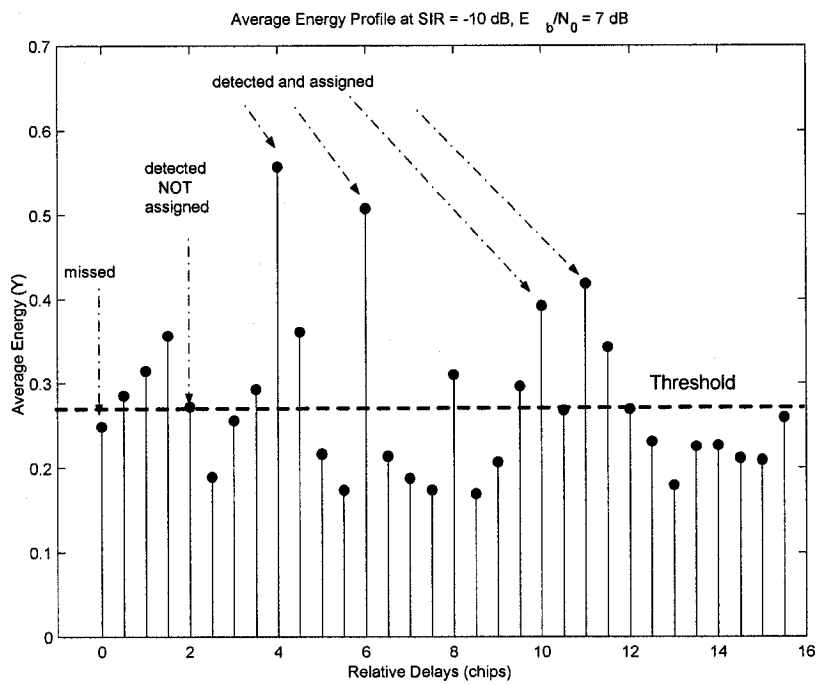

Figure 2.8: Realistic path's average energy profile.

To evaluate the performance of the EMDS we need to find the probability that the detection logic implies that the examined path is correct while it is not, i.e. probability of false alarm, and the probability that the logic indicates that the examined path is correct while indeed it is, i.e. probability of detection. The dependence of these two probabilities on the E_b/N_0, SIR, and the threshold can be sensed from the previous examples. In the following the relationship between these parameters is formulated.

2.2.1 Probability of False Alarm (P_{fa})

Let us assume that the desired user's signal impinges at the receiver front end from L different paths $\{l_1, l_2, \ldots, l_L\}$, with set of delays $\mathbf{d} = \{\tau_1, \tau_2, ...\tau_L\}$. Any of the remaining delay offsets in the search window other than the ones in $\mathbf{d}$ may cause a false alarm. Since the desired user's signal arrives only via the paths $\{l_1, l_2, \ldots, l_L\}$, the probability of false alarm can be calculated from the probability density function (pdf) of the decision metric of the k^{th} delay offset when $\tau_k \notin \mathbf{d}$, that is when the received signal consists of noise and interference only. In this case, the decision metric is given as

$$Y(k) = \tilde{\sigma}_I^2(k). \tag{2.13}$$

It can be shown that $Y(k)$ has a central Chi-square distribution with $2N_A$ degrees of freedom whose pdf is given by [27]

$$f_{Y_k}(y) = \frac{1}{\Gamma(N_A)} \left(\frac{N_A y}{\sigma_I^2(k)} \right)^{N_A - 1} e^{-N_A y/\sigma_I^2(k)}, \quad y \geq 0 \tag{2.14}$$

where $\Gamma(x)$ is the Gamma function defined as $\Gamma(z) = \int_0^\infty x^{z-1} e^{-x} dx$, $z > 0$. The cumulative distribution function (cdf) of $Y(k)$ is then given as [27]

$$F_{Y_k}(y) = 1 - e^{-N_A y/\sigma_I^2(k)} \sum_{i=0}^{N_A - 1} \frac{1}{i!} \left(\frac{N_A y}{\sigma_I^2(k)} \right)^i. \tag{2.15}$$

Using (2.15), the probability that the k^{th} delay offset produces a false alarm state

is

$$P_{fa}(k) = \Pr[Y(k) \geqslant \eta] = e^{-N_A\eta/\sigma_I^2(k)} \sum_{i=0}^{N_A-1} \frac{1}{i!} \left(\frac{N_A\eta}{\sigma_I^2(k)}\right)^i \tag{2.16}$$

We notice from (2.16) that the probability of false alarm increases as the interference power increases. In the existing AAS, the threshold is varied to compensate for any variations in the average interference level, and consequently a CFAR is maintained. However, the selection of the threshold also affects the probability of detection as it will be shown next.

2.2.2 Probability of Detection (P_D)

The probability of detecting a multipath component in the desired user's channel is basically the probability that the average correlation energy corresponding to that component is greater than the threshold. If the desired user's signal impinges at the receiver front end from L different paths $\{l_1, l_2, \ldots, l_L\}$, the average correlation energy corresponding to any one of these paths is given by (2.12). Since the decision metric is a function of two independent random variables, namely $\tilde{p}(k)$ and $\tilde{\sigma}_I^2(k)$, we formulate its conditional pdf as

$$f_{Yk}(y \mid \tilde{p}(k)) = \frac{1}{\Gamma(N_A)} \left(\frac{N_A y}{\tilde{p}(k) + \sigma_I^2(k)}\right)^{N_A-1} \cdot e^{-N_A y/[\sigma_I^2(k)+\tilde{p}(k)]}, \quad y \geq 0 \tag{2.17}$$

and the conditional cdf is

$$F_{Yk}(y \mid \tilde{p}(k)) = 1 - e^{-N_A y/[\sigma_I^2(k)+\tilde{p}(k)]} \cdot \sum_{i=0}^{N_A-1} \frac{1}{i!} \left(\frac{N_A y}{\tilde{p}(k) + \sigma_I^2(k)} \right)^i \tag{2.18}$$

The probability of detecting the $(l_j)^{th}$ multipath component, for $j = 1, 2, \ldots, L$, is given as

$$P_D(l_j) = \int_0^\infty e^{-N_A \eta/[\sigma_I^2(l_j)+\tilde{p}(l_j)]} \cdot \sum_{i=0}^{N_A-1} \frac{1}{i!} \left(\frac{N_A \eta}{\tilde{p}(l_j) + \sigma_I^2(l_j)} \right)^i f_{l_j}(\tilde{p}(l_j)) d\tilde{p}(l_j) \tag{2.19}$$

where

$$f_{l_j}(\tilde{p}(l_j)) = \frac{1}{\Gamma(N_A)} \left(\frac{N_A \tilde{p}(l_j)}{E_{b1}\phi(l_j)} \right)^{N_A-1} e^{-N_A \tilde{p}(l_j)/E_{b1}\phi(l_j)}, \quad \tilde{p}(l_j) \geq 0 \tag{2.20}$$

The expression in (2.20) shows explicitly the effect of the channel PDP on the probability of detection. The deficiency of the EMDS scheme is inferred from the probability of false alarm and probability of detection expressions. It is clear that the probability of detection depends on the total received energy per path $\tilde{p}(l_j) + \sigma_I^2(l_j)$. Consequently, when the interference power is high, the probability of detection and probability of false alarm are proportional to each other. Meaning that trying to maintain a low probability of false alarm by using a high threshold level will retain a low probability of detection as well.

2.2.3 Energy Based Finger Assignment Algorithm

As it has been mentioned before, the finger assignment algorithm works on the search results for all multipath components in the search window. The energy based finger assignment algorithm assuming that there are L fingers in the RAKE is outlined as follows [18].

1. Perform a search over the window of possible delays and obtain the search results at each estimation bit, as per (2.11).

2. Compute the detection metric as per (2.12) .

3. According to the desired false alarm probability, e.g. 1%, the delays with average energy Y greater than the threshold and they are the L maximums among all paths in the search windows are assigned for RAKE combining.

4. In case none of the delays in the current search window exceeds the threshold, the detected delay with maximum Y from the previous search window, corresponding to the previous received frame, is used for demodulation.

5. Repeat this process for each received frame.

2.3 Per-Path Interference Power and Channel Estimation

In this section, a simple per-path interference power estimator is developed and analyzed. The proposed estimator assumes perfect knowledge of the channel fading coefficients during the search instants. Subsequently, a channel estimator based on the knowledge of the channel autocorrelation function is developed. The channel estimation algorithm presented herein, will be used later to realize a low complexity improved multipath detection scheme.

2.3.1 Interference Variance Estimation

To improve upon the energy based detection scheme and finger assignment algorithm, the received per path interference power at the searched delay offsets should be considered. For this purpose, the interference power should be estimated at each delay offset in the search window.

Writing (2.11) in terms of the in-phase and quadrature components, a given sample of the searcher output could be expressed as follows

$$h_k(n) = h_{kI}(n) + jh_{kQ}(n) = \sqrt{p(k)}(\alpha_{1kI}(n) + j\alpha_{1kQ}(n)) + \sqrt{\sigma_I^2(k)}(\bar{I}_I(n) + j\bar{I}_Q(n)). \tag{2.21}$$

Assuming that the in-phase and quadrature components of the interference are

independent, the joint pdf of the in-phase and quadrature components of a sample from the searcher output is given by

$$f(h_{kI}, h_{kQ}|\alpha_{1k}, p(k); \sigma_I^2(k)) = \frac{1}{\pi\sigma_I^2(k)} \times \exp\left(\frac{-g(n)}{\sigma_I^2(k)}\right)$$

where, $g(n) = [h_{kI}(n) - \sqrt{p(k)}\alpha_{1kI}(n)]^2 + [h_{kQ}(n) - \sqrt{p(k)}\alpha_{1kQ}(n)]^2$. Hence the joint pdf of the N_A independent samples can be found to be as follows

$$f(\mathbf{h}_{kI}, \mathbf{h}_{kQ}|\boldsymbol{\alpha}_{1k}, p; \sigma_I^2)) = (\pi\sigma_I^2(k))^{-N_A} \times \exp[\frac{-1}{\sigma_I^2(k)} \sum_{n=1}^{N_A} g(n)]. \tag{2.22}$$

Equation (2.22) represents the Likelihood function for the data model presented above. Taking the natural logarithm of (2.22) yields

$$L(\sigma_I^2(k)) = -N_A \ln(\pi\sigma_I^2(k)) - \frac{1}{\sigma_I^2(k)} \sum_{n=1}^{N_A} g(n). \tag{2.23}$$

The first derivative of (2.23) with respect to the interference variance is

$$\frac{\partial L(\sigma_I^2(k))}{\partial \sigma_I^2(k)} = \frac{-N_A}{\sigma_I^2(k)} + \frac{1}{\sigma_I^4(k)} \sum_{n=1}^{N_A} g(n).$$

Observing that since $\sum_{n=1}^{N_A} g(n) = N_A\sigma_I^2(k)$, the likelihood function satisfies the regularity condition [28] and the its first derivative can be written as

$$\frac{\partial L(\sigma_I^2(k))}{\partial \sigma_I^2(k)} = \frac{N_A}{\sigma_I^4(k)}[-\sigma_I^2(k) + \frac{1}{N_A}\sum_{n=1}^{N_A} g(n)]. \tag{2.24}$$

Hence the Minimum Variance Unbiased (MVU) estimator exits and its variance attains the CRB bound [28]. From (2.24), the estimator can be expressed as

$$\hat{\sigma}_I^2(k) = \frac{1}{N_A}\sum_{n=1}^{N_A} |h_k(n) - \sqrt{p(k)}\alpha_{1k}(n)|^2. \tag{2.25}$$

One the average, the estimate $\hat{\sigma}_I^2(k)$ equals the the actual interference variance $\sigma_I^2(k)$, i.e., $E\{\hat{\sigma}_I^2(k)\} = \sigma_I^2(k)$, where $E\{\cdot\}$ is the expectation operator. Moreover, the variance of the estimator, i.e. the CRB, is given by

$$var\{\hat{\sigma}^2(k)\} = \frac{\sigma_I^4(k)}{N_A} \tag{2.26}$$

As it may be expected, the variance of estimator decreases as the number of independent observations N_A increases. Thus, more accurate estimates of the interference power can be obtained by increasing the number of accumulations. For a given number of accumulations, the variance of the estimator increases as the interference power increases.

Although the interference variance estimator in (2.25) is optimum in the sense

that it is MVU, it assumes perfect knowledge of the desired user's channel coefficients. Clearly, this is rather a strong assumption to hold in practice. In the following, an optimum channel estimator will be developed based on the knowledge of the channel autocorrelation function. The obtained channel estimates can be used in (2.25) instead of the perfect channel coefficients.

2.3.2 Channel Estimation

The task to be carried out here is to obtain optimum estimates of the channel fading coefficients based on the data model constructed by the search results as per (2.21). The sought channel estimator would be optimum in the sense that it minimizes the mean squared error in estimating the fading coefficients at the search instants. Form estimation point of view, it is well known that the Bayesian estimators are the optimum estimators in the mean squared error sense [28]. This is mainly attributed to the fact that the Bayesian estimator assumes knowledge of the pdf of the parameter to be estimated. To derive such an estimator, we need to take a closer look at the data mode presented in (2.21).

In our model, the channel coefficient α_{1k} is complex Gaussian random variable with zero mean and variance 0.5 per dimension. Under the WSSUS channel model, the inphase and quadrature components of any given channel coefficient are uncorrelated, i.e. independent in this case also. The inphase and quadrature components of the

search results can be written separately as

$$h_{kI}(n) = \sqrt{p(k)}\alpha_{1kI}(n) + \sqrt{\sigma_I^2(k)}\bar{I}_I(n), n = 1, 2, ...N_A, \tag{2.27}$$

$$h_{kQ}(n) = \sqrt{p(k)}\alpha_{1kQ}(n) + \sqrt{\sigma_I^2(k)}\bar{I}_Q(n), \ n = 1, 2, ...N_A. \tag{2.28}$$

Since the complex channel coefficient $\alpha_{1k}(n)$ is a linear combination of $\alpha_{1kI}(n)$ and $\alpha_{1kQ}(n)$, i.e. $\alpha_{1k}(n) = \alpha_{1kI}(n) + j\alpha_{1kQ}(n)$, a minimum mean square error (MMSE) estimate $\hat{\alpha}_{1k}(n)$ can be obtained by linearly combining MMSE estimates of the inphase and quadrature components of channel coefficient $\hat{\alpha}_{1kI}(n)$ and $\hat{\alpha}_{1kQ}(n)$, respectively, as $\hat{\alpha}_{1k}(n) = \hat{\alpha}_{1kI}(n) + j\hat{\alpha}_{1kQ}(n)$. Therefore, the estimation problem reduces to estimating the inphase and quadrature components of the fading coefficients.

It is evident that the models in (2.27) and (2.28) are linear models and the underlying processes, i.e., the channel and interference, are jointly Gaussian, the MMSE channel estimates at the search results can be obtained using a linear filter conventionally known as the Wiener filter [28].

If the covariance matrix of the inphase components of the channel coefficient and the interference are denoted by the $N_A \times N_A$ matrices $\mathbf{C}_{\alpha,II}$ and $\mathbf{C}_{I,II}$ respectively, the MMSE estimates of the channel coefficient's inphase component at the search

instants, $n = 1, 2, ...N_A$, can be found as

$$\hat{\boldsymbol{\alpha}}_{1kI} = \mathbf{A}\mathbf{h}_{kI} \tag{2.29}$$

where, $\hat{\boldsymbol{\alpha}}_{1kI}$ and $\mathbf{h}_{kI}$ are column vectors of length N_A containing, respectively, the MMSE inphase channel estimates and the inphase search results, and the Wiener filter matrix $\mathbf{A}$ is given as

$$\mathbf{A} = p(k)\mathbf{C}_{\alpha,II}[p(k)\mathbf{C}_{\alpha,II} + \sigma_I^2(k)\mathbf{C}_{I,II}]^{-1}. \tag{2.30}$$

Having defined the form of the filter, we are left with defining the covariance matrices $\mathbf{C}_{\alpha,II}$ and $\mathbf{C}_{I,II}$. As it has been mentioned previously, the interference component $\bar{I}(n)$ is modeled as an AWGN with zero mean and variance 0.5 per dimension, and the inphase and quadrature components of interference are independent. Therefore, the covariance matrix of the inphase component of the interference samples $\mathbf{C}_{I,II}$ is given as

$$\mathbf{C}_{I,II} = 0.5\mathbf{I} \tag{2.31}$$

where $\mathbf{I}$ is an $N_A \times N_A$ identity matrix.

The covariance matrix of the sampled channel's inphase component, $\mathbf{C}_{\alpha,II}$, can be obtained from the channel autocorrelation function. The autocorrelation function of the of the inphase component of the channel is given as [21]

$$\varphi_{II}(n_T) = 0.5 J_0(2\pi f_d n_T) \tag{2.32}$$

where, $J_0(x)$ is the zero-order Bessel function of the first kind, n_T is the delay index in terms of T_b seconds, and $f_d = f_m T_b$ is the normalized Doppler rate where f_m is the maximum Doppler frequency. As it has been mentioned before, the search instants are spaced in time within the received frame. Effectively, the searcher samples the channel process at a rate of N_A samples per frame. If the samples are spaced uniformly by n_s, $\mathbf{C}_{\alpha,II}$ is constructed from (2.32) as follows.

$$[\mathbf{C}_{\alpha,II}]_{ij} = \varphi_{II}((i-j)n_s) \tag{2.33}$$

where, i and j are the samples' indices, i.e. i and j assume values in $\{1, 2, ...N_A\}$.

With the assumed channel and interference models, the inphase and quadrature components have the same covariance matrix, i.e., $\mathbf{C}_{\alpha,II} = \mathbf{C}_{\alpha,QQ}$ and $\mathbf{C}_{I,II} = \mathbf{C}_{I,QQ}$ [21]. Hence, the same filter is used to estimate the quadrature component of the channel, that is

$$\hat{\boldsymbol{\alpha}}_{1kQ} = \mathbf{A}\mathbf{h}_{kQ}. \tag{2.34}$$

Finally, the complex channel estimates are obtained as

$$\hat{\alpha}_{1k} = \hat{\alpha}_{1kI} + j\hat{\alpha}_{1kQ}. \tag{2.35}$$

Although the estimator in (2.35) is optimum in the sense that it minimizes the mean square error, it relies on the assumption that the interference power and the channel autocorrelation function are known. Because we are mainly interested in estimating the interference power, the Wiener filter solution is rendered unfeasible. In the next section, however, we will use the Wiener filter presented here to propose a more practical filter structure.

2.4 Improved Multipath Detection Scheme (IMDS)

In this section, we present an improved multipath detection scheme based on estimating the interference power seen in the resolved paths. A new detecting metric is formulated by subtracting the estimated interference power from the total power received from each path. This will have the effect of reducing the influence of the interference on the probability of false alarm and probability of detection as we will see later in this section. The properties of the interference variance estimator presented in the previous section will be used to derive the probability of detection and probability of false alarm for the IMDS.

2.4.1 The IMDS Detection Metric

Using the estimates computed from (2.25), the new detection metric is

$$Z(k) = Y(k) - \hat{\sigma}_I^2(k). \tag{2.36}$$

Consequently, under the IMDS, the paths with maximum actual signal power Z will be acquired. Comparing the decision metric given in (2.36) and the one in (2.12), we observe that the proposed metric depends on the desired signal power as opposed to the conventional metric which considers the composite, signal and interference, power in the detection process.

2.4.2 Probability of False Alarm

The detection metric can be written compactly as

$$Z(k) = \tilde{p}(k) + [\tilde{\sigma}_I^2(k) - \hat{\sigma}_I^2(k)]. \tag{2.37}$$

Clearly, the detection metric consists of the signal component $\tilde{p}(k)$ and estimation error given by the term $\tilde{\sigma}_I^2(k) - \hat{\sigma}_I^2(k)$. Since the estimator in (2.25) is MVU, the estimation error is Gaussian distributed with zero mean and variance $\sigma_I^4(k)/N_A$. This is particularly true when the number of search results, i.e. observation samples, is large [28].

Assuming that the desired user channel has L paths with delays set $\mathbf{d} = \{\tau_1, \tau_2, ..., \tau_L\}$,

the probability of false alarm is derived as follows. When the k^{th} searched delay offset does not correspond to a correct path delay, i.e. $\tau_k \notin \mathbf{d}$, the detection metric equals the estimation error, i.e. $\tilde{p}(k) = 0$, and consequently $Z(k) \sim N(0, \sigma_I^4(k)/N_A)$. Using this result, the probability that the estimation error for the k^{th}delay offset exceeds a given threshold ϵ can be found to be

$$P_{fa}(k) = Q\left(\frac{\sqrt{N_A}\epsilon}{\sigma_I^2(k)}\right) \tag{2.38}$$

where $Q(x)$ is the $Q-$function defined as $Q(z) = 1/\sqrt{2\pi}\int_z^\infty e^{-x^2/2}dx$.

2.4.3 Probability of Detection

The probability of detection can be found following the same steps used to find the probability of false alarm. The conditional probability of detecting the $(l_j)^{th}$ multipath component is given by

$$P_D(l_j \mid \tilde{p}(l_j)) = Q\left(\frac{\sqrt{N_A}[\epsilon - \tilde{p}(l_j)]}{\sigma_I^2(l_j)}\right). \tag{2.39}$$

Averaging over the received signal's envelope results in the probability of detecting that component is given by

$$P_D(l_j) = \int_0^\infty Q\left(\frac{\sqrt{N_A}[\epsilon - \tilde{p}(l_j)]}{\sigma_I^2(l_j)}\right) f_{l_j}(\tilde{p})d\tilde{p}. \tag{2.40}$$

It is important to note that while the probability of false alarm at a certain

threshold level depends on the interference power, the probability of detection is a function the received per path signal-to-interference-plus-noise ratio, $\tilde{p}(l_j)/\sigma_I^2(l_j)$.

2.4.4 Practical Realization of the IMDS

Up to this point, we have considered the IMDS based on the MVU interference variance estimates. As it has been pointed out in section 2.3.1, the MVU variance estimator assumes a perfect knowledge of the channel coefficients. At the data demodulation stage, this is a reasonable assumption since the channel coefficients are needed by the RAKE receiver to implement coherent combining of the assigned fingers and a channel estimation algorithm is usually implemented at the receiver for that purpose. At the initial acquisition stage, however, the estimator requires the knowledge of the channel coefficients for all the K delay offsets in the search window. When the search window is large, estimating the channel at each delay offset becomes prohibitive.

In the previous section, the Wiener filter has been introduced as an optimum channel estimator. We have seen that it is required that the interference variance and the channel autocorrelation function be known in order to calculate the filter coefficients. There are two main drawbacks of the Wiener filter solution. First, the channel autocorrelation function should be estimated at the acquisition stage. To estimate the autocorrelation function, long term observations are needed. Hence, the path acquisition will require longer time and more computations. Second, and most importantly, the Wiener filter solution assumes the knowledge of the parameter of

interest for estimation; the variance of the interference.

To account for the hardware limitation of the receiver, a modified low complexity version of the MMSE estimator should be implemented at the detection stage. The Wiener filter structure will serve as design benchmark for the low complexity solution. This can be accomplished as follows.

To obtain an estimate of the interference power, the N_A search results at each delay offset in the search window will pass through an FIR filter to produce 'rough' channel estimates $\tilde{\alpha}_k(n)$. The filtered versions of the search results are given by

$$\tilde{\alpha}_k(n) = \sum_{m=0}^{K_f-1} f(m)h_k(m-n) \tag{2.41}$$

where $f(\cdot)$ is the filter shaping function and K_f is the filter length. Using the filtered search results, a simple per-path interference variance estimator can be expressed as

$$\breve{\sigma}_I^2(k) = \frac{1}{N_A}\sum_{n=1}^{N_A} |h_k(n) - \tilde{\alpha}_k(n)|^2. \tag{2.42}$$

It can be seen that the estimator in (2.42) uses the output of the FIR filter as rough channel estimates in order to estimate the interference variance and the signal power. It is important to notice that other estimators such as the Maximum Likelihood (ML) estimator, which is ought to maximize the likelihood function given in (2.22), may be theoretically employed. However, a search over $2N_A + 1$ variables (the in-phase and quadrature components for all N_A complex channel coefficients in addition to the interference variance) should be conducted at each delay offset by the ML estimator.

Such a computation is highly prohibitive especially at the acquisition stage [25].

In Figure 2.9, we present a schematic diagram of the proposed IMDS structure where the simplified estimator is incorporated into the detection scheme. While the upper branch is used to compute the decision metric of the EMDS, the lower branch is used to estimate the interference variance. It is worth mentioning that the increase in complexity is rather modest compared to the EMDS implementation.

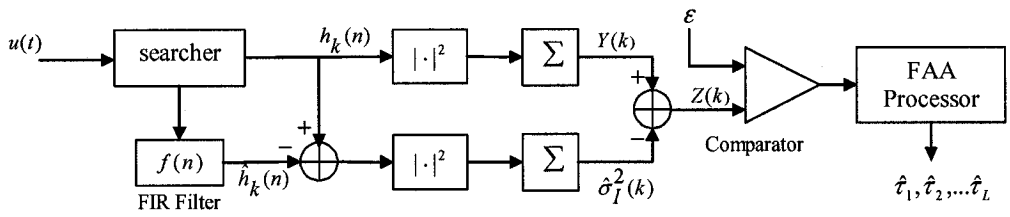

Figure 2.9: A practical realization of the improved multipath detection scheme.

In light of the above discussion, the received signal is first applied to the searcher block. The search results are then used to estimate the per path interference variance using the FIR filter. The decision metric in (2.36) is computed and compared to the threshold. The comparison results are presented to the FAA processing block where the potential paths are chosen for combining.

To highlight the potential of the IMDS on enhancing the detection capability of the multipath components, consider the example where we have 4 paths at 0, 2, 4, and 6 chips. The computed detection metrics for the EMDS and the IMDS at $E_b/N_0 = 7$ dB and $SIR = -10$ along with estimated interference variance are given in Figure 2.10 as a function of the examined delays. The realization in Figure 2.9 has been

used in this example with normalized rectangular window FIR filter of length 6. As shown in Figure 2.10, while the EMDS has not assigned the path at 2 chips (because of the ambiguity resulted from the path at 8.5) , the IMDS has detected and assigned that path. It is evident that the EMDS results in high false alarm rate. This rate is reduced effectively in the case where the IMDS is utilized due to subtracting the interference power seen at each path from the total received path's power.

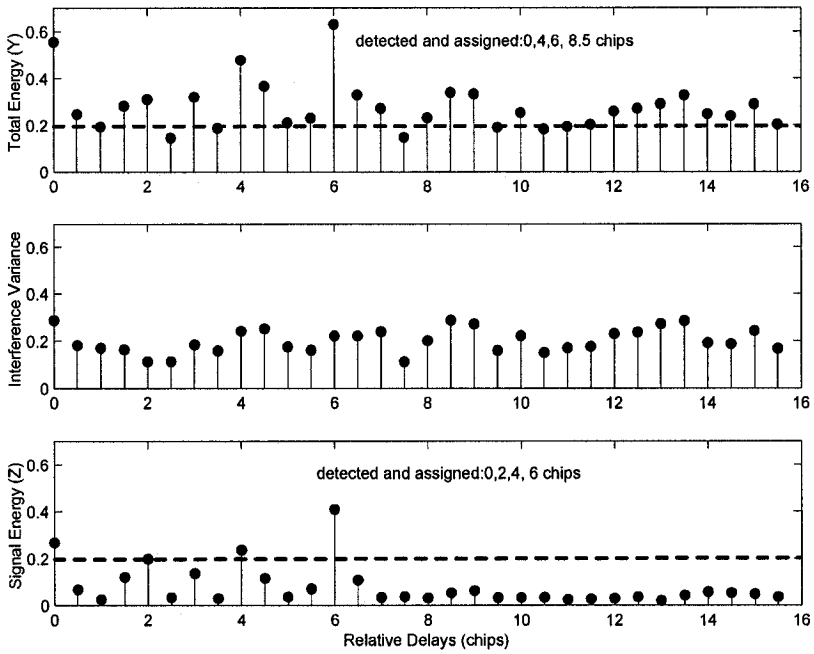

Figure 2.10: The computed total and signal energy profiles with the estimated interference variance as a function of the delays examined by the searcher.

2.4.5 The FIR Filter Design Procedure

Herein, a procedure to design the FIR filter used to provide coarse channel estimates in the low complexity realization of the IMDS is described. More specifically, the

filter shaping function and the filter length will be determined using the Wiener filter as a design benchmark.

First let us focus on the filter shaping function. As shown in equation (2.30), the shape of the Wiener filter is drawn by the covariance matrix of the interference and the channel. In reality, the interference power is unknown, and the channel autocorrelation function is very complex to estimate. Hence, the Wiener filter structure can not provide us with a realistic filter shape to implement. Consequently, we adopt a normalized rectangular window FIR filter, i.e., $\sum_{m=0}^{K_f-1} |f(m)|^2 = 1$.

Having defined the filter shape, we are left with one degree of freedom; the number of filter taps K_f. As it can be inferred from the Wiener filter, the number of filter taps depends on the number of the search results N_A and the normalized Doppler rate. In a fixed frame length, when the number of the search results is small, and the Doppler rate is high, the Wiener filter can be approximated by

$$\mathbf{A}_a = \frac{p(k)}{p(k) + \sigma_I^2(k)}\mathbf{I}. \tag{2.43}$$

In this case, the channel estimates would be equal to the search results scaled by $\frac{p(k)}{p(k)+\sigma_I^2(k)}$. Thus, the current estimates depends on the current search result, i.e. the filter becomes memoryless. Consequently, a rectangular FIR filter with small number of taps is expected to provide acceptable performance compared to the Wiener filter.

By increasing N_A or decreasing the Doppler rate, off-diagonal terms will appear in the Wiener filter matrix, and hence, the current estimate will be calculated from some

of the previous and next search results. In particular, the search results which are highly correlated will affect each other. In this case, the number of the rectangular FIR filter taps should be increased to account for the correlation between the search results.

Finally, for a given large N_A, if the Doppler rate is high, the number of the FIR filter taps must be decreased in order to assure sufficient averaging of the interference while the channel is varying rapidly. This implies that the number of filter taps should be selected such that the time span of the filter be proportional to the channel coherence time, i.e. the inverse of the Doppler bandwidth.

Although adapting the number of filter taps according to the Doppler rate for a given number of search results is a possible solution, it requires estimating the Doppler rate at the acquisition stage, which in turn, adds extra complexity at the receiver side. To avoid any additional complexity, it is always desirable to have a fixed design for the FIR filter. To this end, the following steps are customized, taking into consideration the comparison with Wiener filter, to furnish the desired filter.

1. Since we don't know the interference variance at each delay offset (so we can not calculate the Wiener weights even if we know the channel covariance matrix), we adopt a normalized rectangular window FIR filter of length K_f with impulse response given by

$$f(n) = \frac{1}{\sqrt{K_f}} \sum_{i=0}^{K_f-1} \delta(n - iT_b) \tag{2.44}$$

where $\delta(t)$ is the dirac delta function.

2. Assuming that the channel is known, the number of search results N_A is fixed to yield a certain detection performance (as predicted by equations (2.38) and (2.40)). N_A, however, should not be selected arbitrary large since that would increase the delay acquisition time.

3. The number of taps for $f(n)$ should be selected upon comparing the performance with the Wiener filter. The best strategy is to select the taps that would make the detection performance with $f(n)$ as close as possible to the Wiener filter performance when the Doppler is high. This will work well even when the Doppler rate is low since the search results are spaced in time.

In the next section, we will show that this strategy results in a good performance under most realistic channel conditions.

2.4.6 Finger Assignment Algorithm Based on the IMDS

Having defined the detection decision metric of the IMDS in (2.36), the IMDS based finger assignment algorithm assuming that there are L fingers in the RAKE is outlined as follows.

1. Perform a search over the window of possible delays and obtain the search results at each estimation bit, as per (2.11).

2. Compute the detection metric as per (2.36).

3. According to the desired false alarm probability, e.g. 1%, the delays with signal power Z greater than the threshold are detected.

4. The delays with maximum L signal power Z values among all the detected paths in the search windows are assigned for RAKE combining.

5. In case none of the delays in the current search window exceeds the threshold, the detected delay with maximum Z from the previous search window, corresponding to the previous received frame, is used for demodulation.

6. Repeat this process for each received frame.

2.5 Numerical Results and Discussion

In this section, we examine the performance of a CDMA receiver when multipath detection and finger assignment are performed based on the detection schemes described and developed in the previous sections; the EMDS and the IMDS. As it has been seen from the description of the multipath detection problem in general, there are many design parameters which should be considered in various operational environments in order to draw conclusive remarks about the performance of the receiver. As far as the performance of the CDMA receiver is concerned, we will confine ourselves to a set of performance measures. Mainly, we will study the receiver performance in terms of the operational characteristics, i.e. probability of detection and probability of false alarm,

and the transmission reliability represented by the bit-error rate (BER). The communication environment's and the multipath detection scheme's design parameters pertaining to the adopted performance measures will be considered herein.

2.5.1 System Parameters

An uplink CDMA system similar to the one proposed by the cdma2000 standard was simulated in the baseband. The simulation setup for the system, transmitter, channel, and the receiver parameters are as listed below.

- System: The system consists of a total of 6 (1 desired and 5 interferers) asynchronous users communicating with a single BS, and each mobile terminal transmits its own pilot channel. Perfect power control is assumed, and hence, the 5 interferers' signals arrive at the BS with equal power.

- Transmitter: Each user is assigned a distinct pseudorandom (PN) code of length $N_c \in \{32, 128, 256\}$. The BPSK modulated data bits are spread by a Walsh code before they are code-multiplexied with the pilot channel. A rectangular pulse is used to shape the transmitted chips. The pilot channel gain Gp is set to -3 dB relative to the traffic channel, i.e. $G_P = 0.5E_b$. The transmitted average bit energy is normalized to 1. The frame duration is 20 ms which consists of 192 bits at a data rate of 9600 bps.

- Channel: A frequency selective Rayleigh fading channel is considered here. the Doppler spectrum of the channel follows the classic (outdoor) model as given

in equation (2.32) where the normalized Doppler rate $f_d \in \{10^{-2}, 10^{-3}, 10^{-4}\}$. The number of paths L is set to 4 at relative delays $\mathbf{d} = \{0, 2, 4, 6\}$ chips with uniform power delay profile, i.e. $\phi(l) = 1/4$.

- Receiver: The receiver structure described in section 1 is used in this simulations with following parameters.

    1. Searcher: The search step size S is set to one-half a chip. The search uncertainty region C spans a total of $16T_c$ seconds. Thus, the uncertainty region consists of $K = 32$ delay offsets.

    2. Multipath Detection and FAA: Both the IMDS and EMDS will be considered. Unless specified otherwise, the practical realization of the IMDS shown in Figure 2.9 is utilized with normalized rectangular FIR with $K_f \in \{3, 6, 9\}$.

    3. RAKE: The RAKE receiver consists of L fingers. If the number of detected and assigned paths is less than the number of available fingers, the vacant fingers are switched off. For each assigned delay, the channel is estimated using a moving average rectangular filter of length 6.

The average bit energy-to-noise power spectral density (E_b/N_0) is defined at the output of the despreader. The considered E_b/N_0 varies from 0 to 10 dB. The signal-to-interference ratio (SIR), on the other hand, is defined before despreading. Hence, the measured SIR after despreading SIR_m, in dB, would be approximately the set

SIR in dB plus the processing gain in dB. That is, $SIR_m = SIR + 10\log(N_c)$. Herein, $SIR \in \{-10, 0, 10\}$ dB.

Finally, the developed simulation environment allows for easy access to the received signal components at the receiver (so that we can measure the actual interference power for instance). The simulation environment has been built entirely using MATLAB.

2.5.2 Validation

In the analysis given in sections 2 and 4, some approximations have been made in order to pin down expressions for the probability of detection and probability of false alarm for the EMDS and IMDS. In the following, the validity of the adopted approximations is assessed by comparing the theoretical and simulation results.

For the EMDS, it has been assumed that the average signal power and interference variance, measured at the output of the despreader as $\tilde{\sigma}_I^2(k)$ and $\tilde{p}(k)$, have distributions that can be approximated by central Chi-square distributions with $2N_A$ degrees of freedom. The first and second order statistics of these variables have been given as

$$\begin{aligned} E\{\tilde{\sigma}_I^2(k)\} &= \sigma_I^2(k), \\ var\{\tilde{\sigma}_I^2(k)\} &= \frac{\sigma_I^4(k)}{N_A}, \\ E\{\tilde{p}(k)\} &= p(k), \text{ and} \\ var\{\tilde{p}(k)\} &= \frac{p^2(k)}{N_A}. \end{aligned}$$

As a sample scenario, let's consider the simulation results when $N_A = 24$, $N_c = 128$, $f_d = 0.01$, $SIR = 0$ dB, and $E_b/N_0 = 0$ dB. For the first path, $\sigma_I^2(1) = 1+1/N_c = 1.0078$ and $p(1) = (1/L)(0.5) = 0.125$. Table 2.1 compares the distributions' first and second order statistics as expected from the equations above against their empirical counterparts. It is evident that the theoretical results are in good agreement with the corresponding empirical results.

Table 2.1: EMDS: emperical versus approximation.

	Approximation	Empirical
$E\{\tilde{\sigma}_I^2(1)\}$	1.0078	1.0028
$var\{\tilde{\sigma}_I^2(1)$	0.0423	0.0418
$E\{\tilde{p}(1)\}$	0.125	0.1248
$var\{\tilde{p}(1)\}$	6.510×10^{-4}	6.6251×10^{-4}

To evaluate the validity of distribution approximation, the probability of detecting the first path as expected from equation (2.19) is plotted in Figure 2.11 against the threshold values at the operational parameters mentioned above. In same graph, the empirical counterpart is also depicted.

The probability of detection is selected as the assessment measure since it depends on both pdf approximations. As it is shown in the figure, there is almost an exact match between the theoretical and empirical results. This is explained in terms of the underpinning condition for the pdf approximation. As it has been mentioned in section 2, the pdf approximation holds well when the time-bandwidth product $N_A T_d/T_c$ is large. Observing that dwell time $T_d = T_b = N_c T_c$, the time-bandwidth product evaluates to $N_A N_c = 3072$. It is clear that the time-bandwidth product is large enough for the approximation to hold. Fortunately, this is true for most

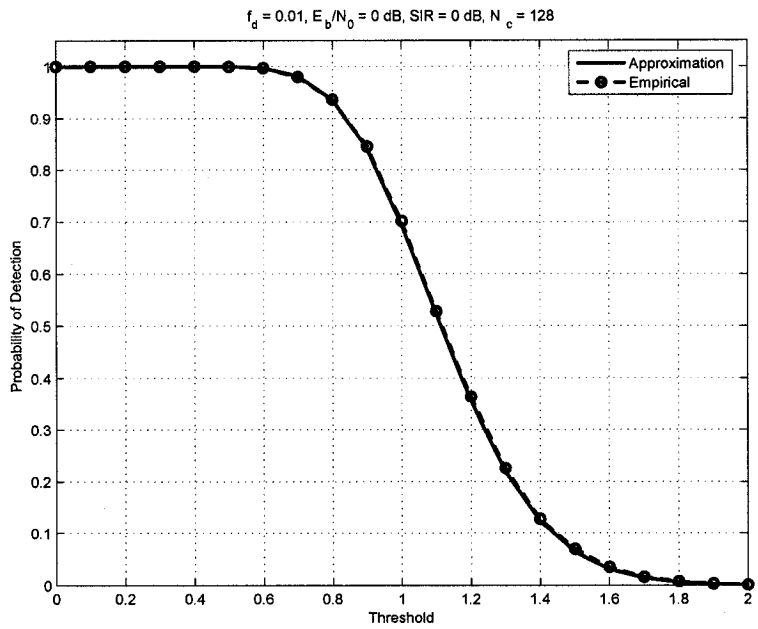

Figure 2.11: The theoretical probability of detection for the first path compared to the one produced by simulations.

practical values for N_A, T_d, and T_c [22] [26].

For the IMDS, a higher level of approximation has been used to derive the probability of detection and probability of false alarm. Beside the approximations adopted for the EMDS, the IMDS assumes that the error in estimating the interference variance possesses a Gaussian pdf with zero mean and variance $\sigma_I^4(k)/N_A$. It is imperative that N_A be sufficiently large for the Gaussian approximation to apply. To assess this approximation, Table 2.2 lists the theoretical mean (0) and variance $(\sigma_I^4(1)/N_A)$ of the estimation error against their empirical counterparts for the same operational parameters used above.

As shown in Table 2.2, the theoretical first and second order statistics compare well

Table 2.2: IMDS: emperical versus approximation.

	Approximation	Empirical
$E\{\sigma_I^2(1) - \hat{\sigma}_I^2(1)\}$	0	-4.8627×10^{-6}
$var\{\sigma_I^2(1) - \hat{\sigma}_I^2(1)\}$	0.0423	0.0443

with their empirical counterparts. However, the variance produced in the simulations appears to be a bit larger than the one expected theoretically. To further investigate this case, the pdf of the estimation error as produced from the simulations is plotted in Figure 2.12 against a Gaussian distributed random variable (RV) with mean equal to zero and variance of 0.0423.

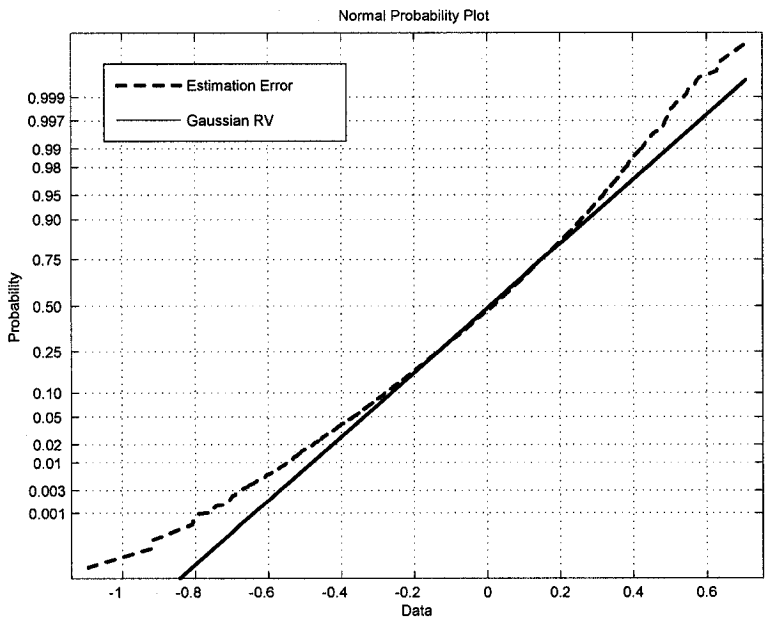

Figure 2.12: The estimation error pdf as it compares to a Gaussian distributed random variable.

It is clear that estimation error pdf flares in at the tail probability. This basically makes the variance increase. Except for the tail probabilities, the approximation holds quite well. By the virtue of the condition behind the approximation, increasing

the number of search results N_A beyond 24 will insure a better match between the theoretical and empirical results.

To highlight the impact of the Gaussian approximation on the probability of detection, the probability of detecting the first path as computed from equation (2.40) is plotted in Figure 2.13 against the results produced by simulations.

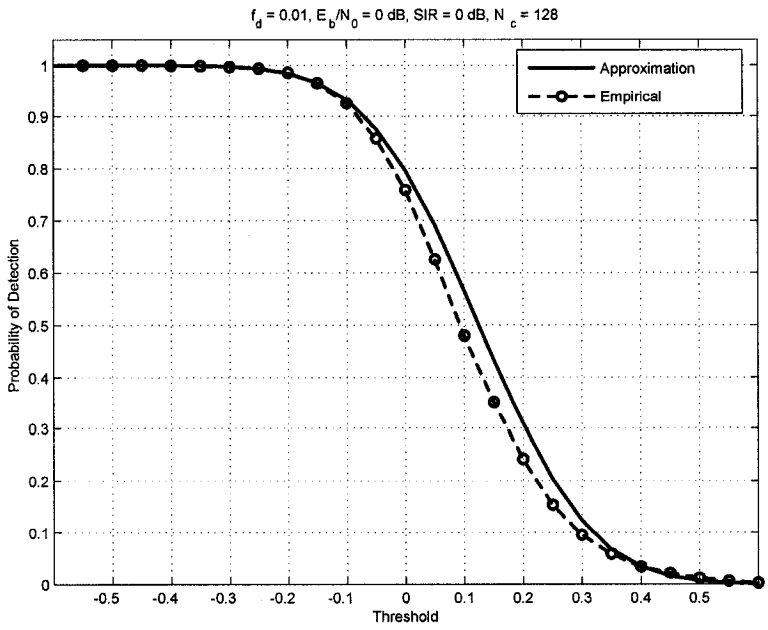

Figure 2.13: The theoretical probability of detection for the first path using the IMDS as it compares to its simulation counterpart.

Immediately apparent is the fact that, for high probability of detection, the theoretical results agree very well with the empirical results. The effect of the aforementioned mismatch is practically negligible as shown in Figure 2.13.

2.5.3 The Receiver Operational Characteristics (ROC)

The most informative performance assessment aids for any detection scheme is the receiver operational characteristics (ROC) curves. In the ROC curve, the probability of detection is plotted against the probability of false alarm at certain operational parameters. The ROC curves are typically produced via off-line calibration processes. During these processes, the threshold level is varied, and thereupon the probability of detection and probability of false alarm at each threshold level is measured. In the forthcoming discussions, the ROC curves will be investigated in various communication environments.

To illustrate the detection performance improvement provided by the IMDS when the FIR filter length K_f is varied with the Doppler rate, the ROC curves are produced at different Doppler rates for both detection schemes. The filter length K_f is increased when the Doppler rate decreases. The used adaptation scheme is described by the set $\{(f_d, K_f) : (10^{-2}, 3), (10^{-3}, 6), (10^{-4}, 9)\}$. As sample results, consider Figure 2.14 which shows the ROC curves, i.e. the probability of detecting the first path as a function of the probability of false alarm, for both detection schemes at $E_b/N_0 = 8$ dB, $SIR = -10$ dB when $N_c = 128$ and $N_A = 24$.

From the above figure, it is seen that, for the same Doppler rates, the IMDS results in higher detection probability than the EMDS. For instance, at $P_{fa} = 1\%$, the IMDS is capable of detecting the first path at least by more than 20% of times compared to the EMDS at all Doppler rates. It is also evident that the detection capabilities for both detection schemes deteriorate as the Doppler rate decreases. This is mainly

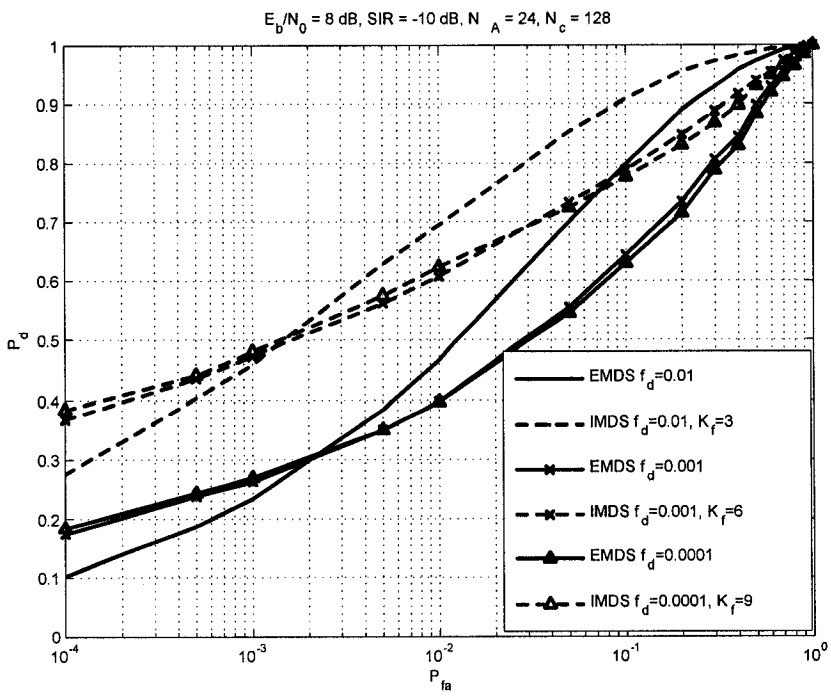

Figure 2.14: The ROC for the EMDS and IMDS when the FIR filter length changes with the adaptively Doppler rates.

because the search results becomes more correlated at lower Doppler rates, and hence, the search samples provide similar information about the energy content of the path. Given that the probability of deep fade in the path is high, the information provided by the search results are typically not indicative. One possible strategy to remedy this situation for both detection schemes, is to further time-space the search results. This, however, will increase the finger acquisition time for fixed N_A (a search over more than one frame is needed). Another solution, is to decrease the number of search results within the frame. As it may be expected, the drawback of this solution is that the probability of detection will decrease.

As mentioned in section 4, the practical realization of the IMDS can be implemented with a fixed FIR filter design, i.e. with fixed K_f, by direct ROC comparisons with the optimum Wiener filter described in section 3. To put the developed FIR design strategy in practice, the detection performance of the IMDS when the channel coefficients are perfectly known is computed with $N_A = 24$ to yield a certain detection performance. With the same system parameters, the detection performance of the EMDS and the IMDS implemented once with the Wiener filter and once again with the normalized rectangular FIR filter with $K_f = 3$ is evaluated. Sample results of the ROC comparisons are shown in Figure 2.15 at $E_b/N_0 = 0$ dB, $SIR = 0$ dB, $N_c = 128$, and $f_d = 0.01$.

The performance gap between the cases when the channel is perfectly known and when the Wiener filter and the rectangular FIR implementations are used is clearly shown to be large. Later in this chapter, the potential of this gap on the BER performance will be demonstrated. The performance improvement gained by the Wiener and the rectangular FIR implementations of the IMDS compared to the EMDS is also shown in the figure. Most importantly, the performance gap between the (optimum) Wiener and the designed FIR realizations of the IMDS is very narrow. From Figure 2.15, it can be concluded that the rectangular FIR realization with $K_f = 3$ performs well compared to the Wiener realization.

To illustrate the robustness of the designed FIR against Doppler rate variations, the probability of detecting the first path is plotted in Figure 2.16 as a function of the normalized Doppler rate for the Wiener filter realization of the IMDS, the rectangular

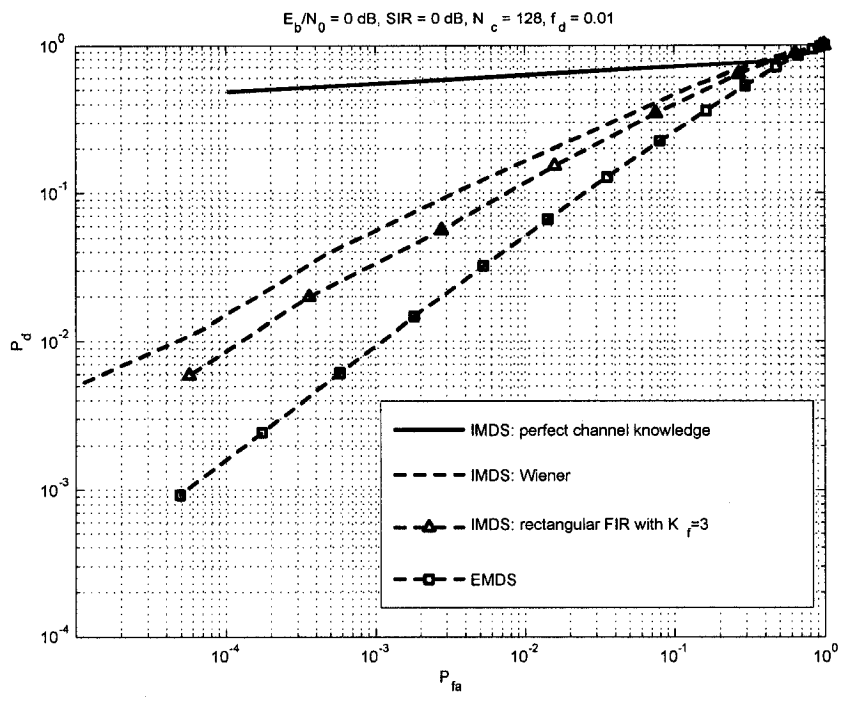

Figure 2.15: The ROC comparisons between the EMDS and the IMDS when: the channel is known, estimated by a Wiener filter, and roughly estimated by the designed FIR with $K_f = 3$.

FIR filter IMDS realization with $K_f = 3$, and the EMDS at fixed probability of false alarm of $P_{fa} = 0.01$. The other system parameters are shown on the top of the graph.

As shown in the above figure, the IMDS realization with rectangular filter with $K_f = 3$ follows the performance trend of the Wiener filter even at Doppler rates other that the one it has been design at, i.e. $f_d = 0.01$. It is also observed from Figure 2.16 that the rectangular FIR realization of the IMDS maintains a superior performance compared to the EMDS in the whole range of Doppler rates. The FIR realization of the IMDS draws a detection performance that is higher than the EMDS's at least by 15% at all Doppler rates.

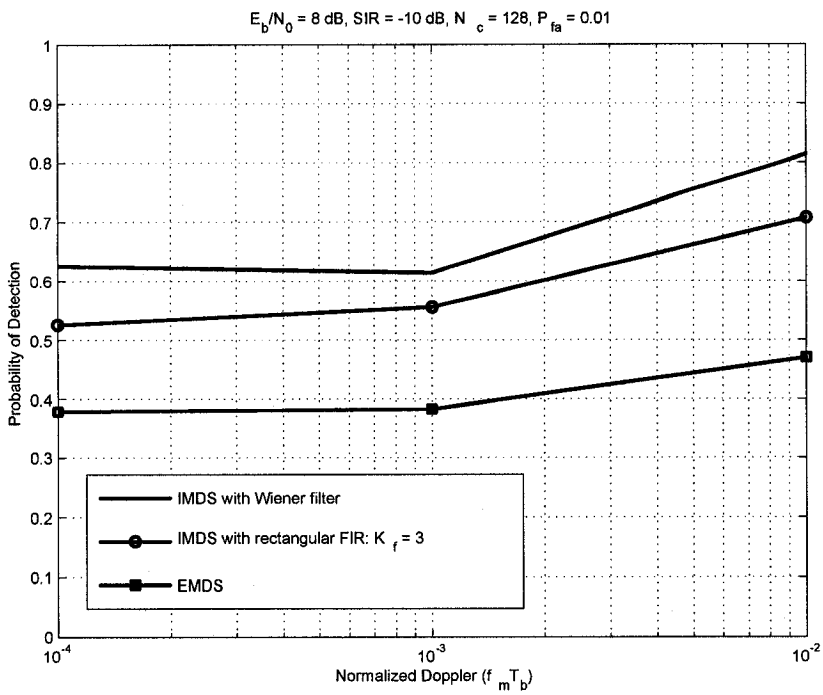

Figure 2.16: The probability of detection as a function of the normalized Doppler rate.

These results demonstrate the efficacy of the fixed design procedure adopted here to realize a feasible version of the IMDS. Considering the complexity of the Wiener filter realization, the performance shown by the rectangular filter with the fixed design makes it a prominent candidate for deployment. From now on, the IMDS implemented with rectangular filter of length 3 will be used.

Finally, since some of the current 3G CDMA systems utilize a variable spreading factor schemes to support different data rates, it becomes a critical issue to investigate the detection performance of the EMDS and the IMDS with different spreading factors. Figure 2.17 shows the ROC curves of the IMDS and EMDS for different N_c; 32, 128, and 256. These values, respectively, correspond to approximate processing

gains of 15, 21 and 24 dB. The other parameters are listed on the top of the graph.

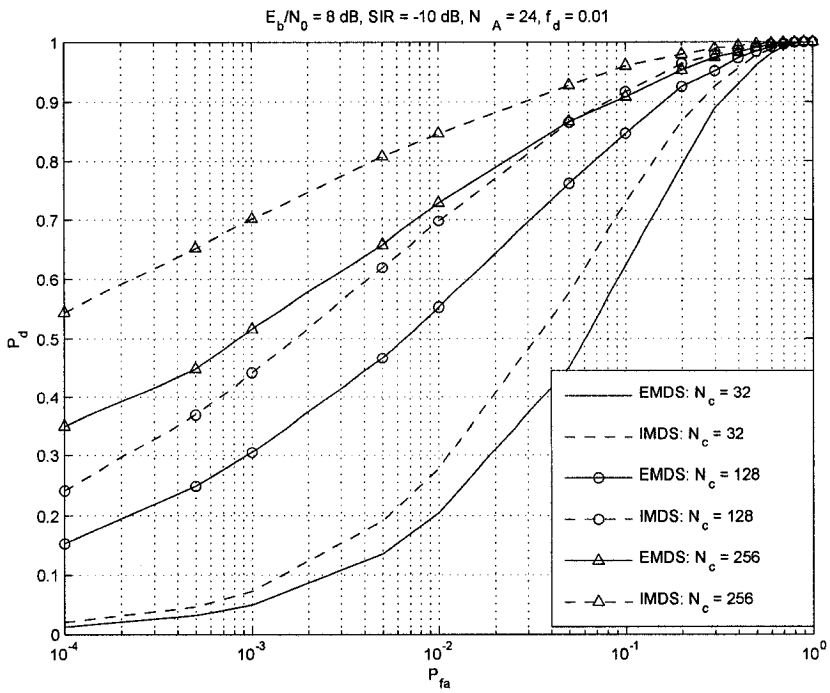

Figure 2.17: The ROC for the EMDS and IMDS with spreading factors; 32, 128, and 256.

It is apparent that the detection performance, for both schemes, is directly proportional to the processing gain. This is mainly because the processing gain determines, actually scales down, the interference power at the output of the despreader. Hence, at low spreading factor as 32, the detection performance deteriorates severely. However, the IMDS maintains a performance improvement in the range of $8 - 12\%$ for the considered processing gains compared to the EMDS when the probability of false alarm is set around 0.01.

After examining the performance of both detection schemes in terms of their

capabilities of detecting a certain path under various operational environments, investigating the RAKE finger assignment performance drawn by both schemes is in order.

2.5.4 Finger Assignment Performance

As it has been explained in sections 2 and 4, the detected paths with maximum decision metric values are allocated to the vacant RAKE fingers. In this section, we compare the finger assignment algorithm (FAA) performance when it is based on the EMDS and the IMDS. The performance measure adopted herein is the average probability that the assignment algorithm assigns the correct path, from the desired user's channel, to a RAKE finger. This probability is henceforth called the Probability of Accurate Assignment (PAA).

As an illustration, Table 2.3 lists the assigned delays (in chips) by both assignment strategies for ten frames at $E_b/N_0 = 0$ dB, $SIR = 0$ dB, when $N_c = 128$, $N_A = 24$, $f_d = 0.01$, and the probability of false alarm is set to 0.01. As it has been mentioned at the beginning of this section, the actual delay set in chips is $\mathbf{d} = \{0, 2, 4, 6\}$. A delay of -1 chip indicates that no potential path is found.

Although the per-frame assignment results do not allow for conclusive remarks about the average assignment performance be drawn, they indicate that the IMDS would provide a certain improvement in terms of finger assignment.

In order to gain further insight on the actual assignment performance, the average probability of accurate assignment needs to be studied. Figure 2.18 shows the PAA

Table 2.3: Sample finger assignment results.

EMDS based FAA	IMDS based FAA
$2, 10, 0, 13$	$2, 5, 9, 1$
$2, -1, -1, -1$	$2, -1, -1, -1$
$8, -1, -1, -1$	$1, -1, -1, -1$
$8, -1, -1, -1$	$2, -1, -1, -1$
$8, -1, -1, -1$	$2, -1, -1, -1$
$8, -1, -1, -1$	$2, -1, -1, -1$
$8, -1, -1, -1$	$2, -1, -1, -1$
$4, -1, -1, -1$	$6, 4, 15, -1$
$4, -1, -1, -1$	$6, -1, -1, -1$
$10, -1, -1, -1$	$2, 6, -1, -1$

of the first path as a function of E_b/N_0 at different values of SIR based on both detection schemes. The probability of false alarm is set to 1% for both schemes.

As we have pointed out before, the EMDS scheme suffers from severe degradation at low E_b/N_0 for all values of SIR. On the other hand, the IMDS exhibits a better performance over the entire range of E_b/N_0 and SIR. This is again because the IMDS takes into consideration the effect of both the interference and noise in the detection process.

For diversity combining, the probability of accurately finding all the multipath components is very important as it impacts the diversity order in the error rate performance. This probability is depicted in Figure 2.19 as a function of E_b/N_0 at different SIR for both detection schemes.

As shown in Figure 2.19, the IMDS maintained a superior performance with respect to the EMDS. Although at low E_b/N_0 the PAA is poor, the performance improves exponentially as E_b/N_0 increases. Also, it can be observed that the IMDS results in a gain that ranges from 3 dB (at low SIR) to 2 dB (at large SIR) for

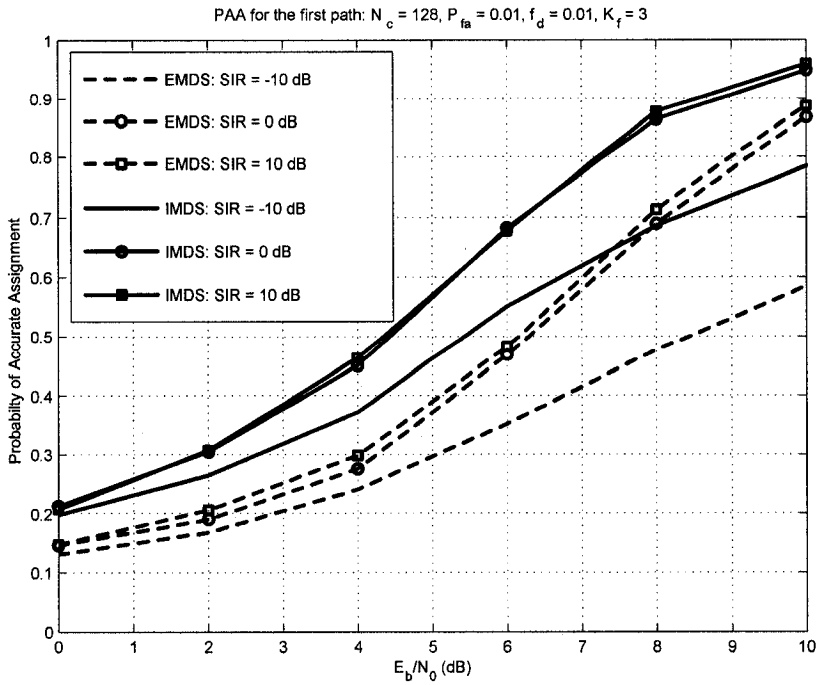

Figure 2.18: The probability of accurately assigning the first path by the EMDS and EMDS based FAA.

large values of E_b/N_0. This gain essentially suggests that the IMDS is more efficient in utilizing the pilot channel's power. This means that, as long as the assignment performance is concerned in the realistic systems (which operates at low SIR), the IMDS with 0.5 of the pilot power used by the EMDS, will draw the same assignment performance as the EMDS . The potential of this gain on the power consumption of the mobile terminal, which typically has limited power resources, is promising.

2.5.5 BER Performance

The impact of multipath detection and finger assignment on the average bit-error-rate performance is investigated in the following. For this purpose, the BER performance

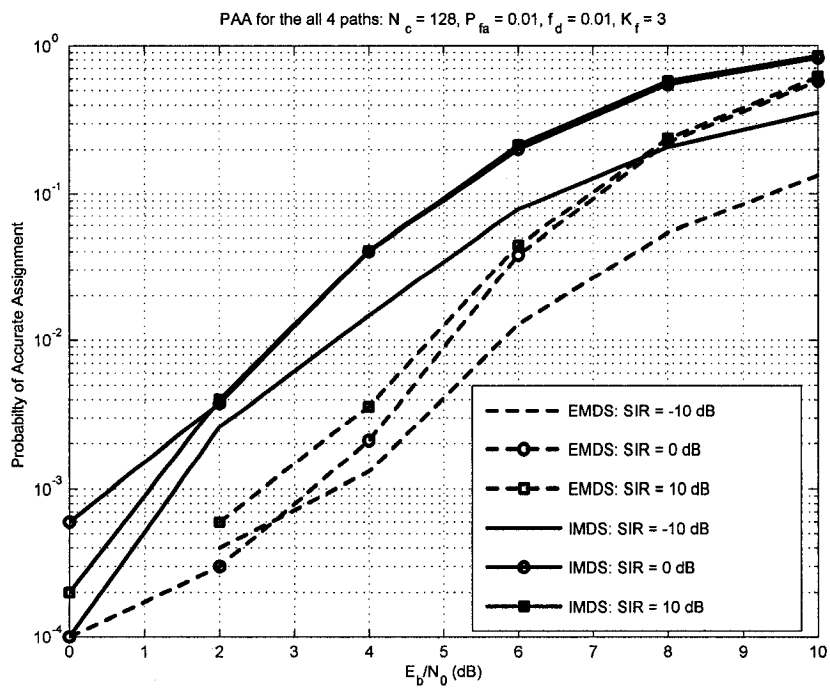

Figure 2.19: The probability of accurately assigning the 4 paths by the EMDS and EMDS based FAA(s).

of the RAKE receiver when the delays are perfectly known[3], assigned based on the EMDS, and when they are assigned based on the IMDS is studied.

Figure 2.20 shows the above mentioned curves as functions of E_b/N_0 at $SIR = -10$ dB, $N_c = 128$. The other system parameters are listed on the top of the graph.

Immediately apparent is that the BER performance gap between the case when the delays are known and when they are assigned based on EMDS is quite large (around 4 dB at high E_b/N_0). This gap shrinks to almost 2.5 dB when the IMDS is utilized to allocate the RAKE fingers. Hence, it is evident that the IMDS results in a

[3]But the channel coefficients seen at those delays are not known, they are estimated as mentioned at the begining of the section.

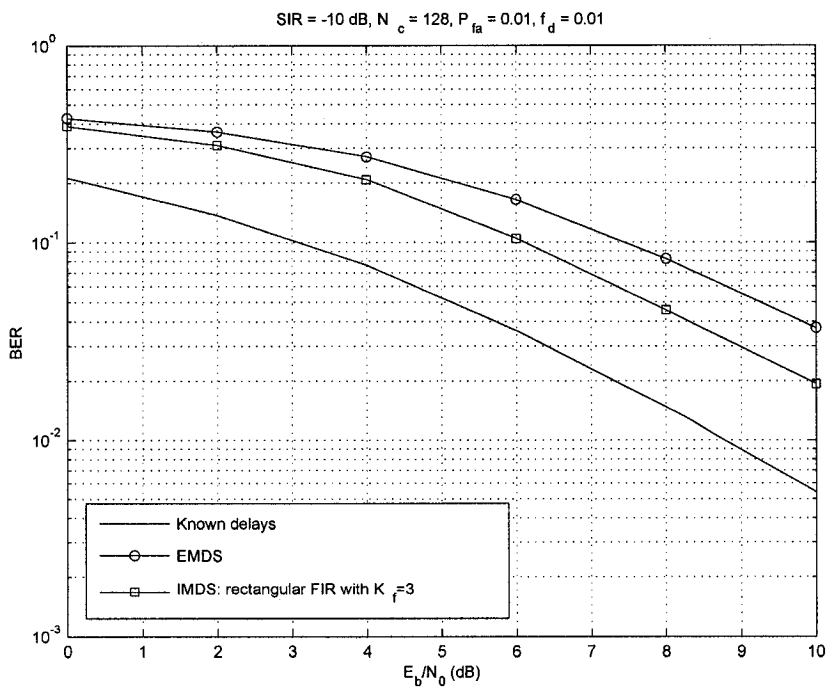

Figure 2.20: The BER performance when $N_c = 128$.

considerable performance gain as compared to the EMDS. As shown in the figure, a gain of around 1.5 dB in E_b/N_0 is realizable when finger assignment is conducted based on the IMDS as opposed to the EMDS. This gain is justified by the superior detection and assignment performance drawn by the IMDS as it has been demonstrated in the previous sub-sections.

The effect of the reduction in the processing gain on the BER performance of the RAKE receiver can be examined by the aid of Figure 2.21. In this figure the BER performance for the same cases mentioned above is presented when the spreading factor is set to 32.

Since reducing the processing gain has the effect of the increasing the interference

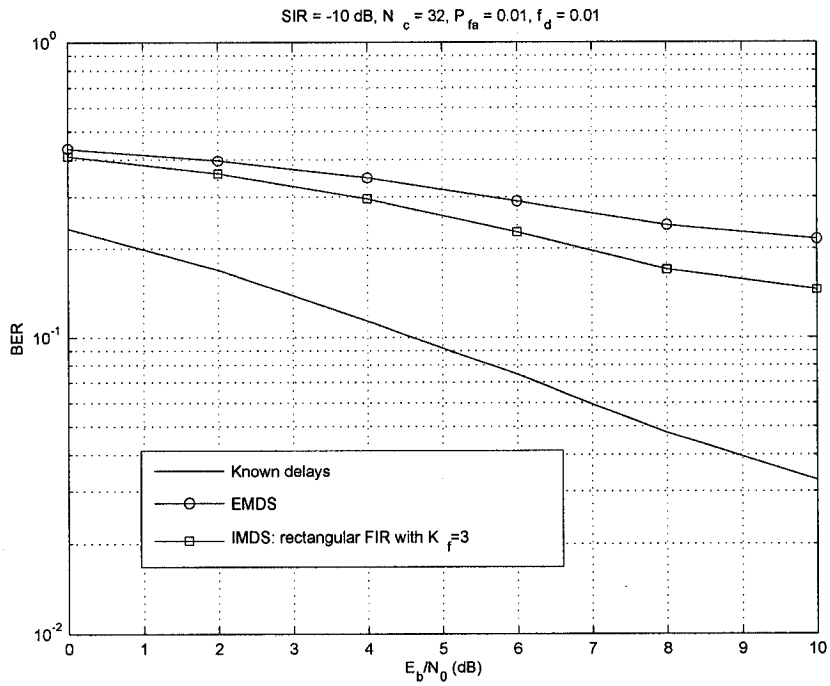

Figure 2.21: The BER performance when $N_c = 32$.

level at the output of the combiner, the BER performance deteriorates even when the delays are perfectly known. Nevertheless, the IMDS has shown a better performance as compared to the EMDS. At large E_b/N_0, the IMDS provides a gain of more than 3 dB compared to the EMDS.

The results shown here, and with an eye on the simplicity of the IMDS, once again suggest that the IMDS constitutes a prominent candidate for deployment.

2.5.6 On the Delay Resolution of the EMDS and IMDS

As a matter of fact, the EMDS and IMDS are both based on a passive correlation search. Hence, these schemes offer low path resolution as compared to the MUltiple

SIgnal Classification (MUSIC) and ML techniques [25] [29] [30]. Both schemes fail to detect paths that are within a chip. Actually, they can only detect two paths when the inter-path delay is greater or equal to the chip duration [31]. This is mainly because of the autocorrelation behavior of the used pseudorandom codes.

To illustrate the resolution capability of IMDS and EMDS, the noise and interference free average search energy delay profile is examined when there are two paths that are separated by a chip duration or less. Figure 2.22 shows the search profile averaged over many channel realizations when there are two paths that are spaced by 0.25, 0.5, and 1 chip in the channel.

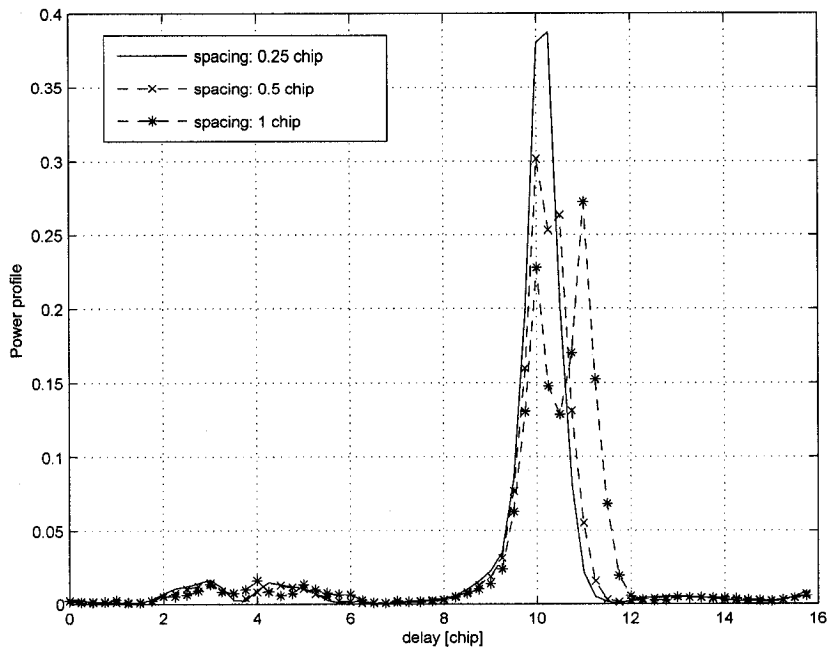

Figure 2.22: The delay profile for different inter-path spacing.

As shown in the figure, two peaks will be resolved only when the inter-path delay spacing is in the order of the chip duration. This is observed for the paths when they

are placed at delays of 10 and 11 chips.

For practical systems, however, the promising resolution attained by MUSIC and ML is not utilized since these techniques are prohibitively complex to realize [30]. Thus, the current systems utilize the EMDS followed by a DLL to resolve fractionally spaced delays if ever needed. In this structure, the IMDS can replace the EMDS with moderate additional complexity.

2.6 Conclusions

In this chapter, the problem of multipath detection for CDMA systems has been tackled. The energy based multipath detection scheme has been described and assessed. We have presented an improved multipath detection scheme to boost the system performance. With the proposed scheme, the multipath detection is modified such that the interference component is taken into account in detecting and assigning the potential multipath components to the RAKE fingers.

The performance of the proposed scheme has been analyzed and compared with that of the energy-based scheme. We have shown that the proposed scheme outperforms the conventional one in different ways. In terms of the probability of detection and probability of false alarm, the proposed scheme has shown a great potential in enhancing the receiver operational characteristics. Also, the proposed scheme has proved to be more efficient as it improves the bit error rate performance and requires less pilot power.

Chapter 3

Multipath Detection for CDMA Systems with Space-Time Spreading

In this chapter, we address the problem of multipath detection as it applies for CDMA systems that employ space-time spreading (STS). As was shown in the previous chapter, the multipath components are detected and assigned to the RAKE fingers based on their average energy content, i.e. the EMDS. It will be shown that the errors produced by the conventional scheme in detecting the potential multipath components severely impact the performance of the receiver. To boost the performance, we utilize the improved multipath detection developed earlier for the conventional CDMA systems. The results show that the proposed scheme not only improves the BER performance significantly but also utilizes the pilot power more efficiently.

3.1 Introduction on STS

Transmit diversity techniques constitute promising means to compact slow fading in mobile communication systems. Among all, open loop transmit diversity techniques are particularly appealing to the system designer as they do not reduce the uplink capacity by feeding the base station back with the channel information. Recently, a space-time spreading (STS) scheme has been included into the Third Generation (3G) cdma2000 standard as an open loop transmit diversity with two transmitter antennas and one receiver antenna option. The STS scheme has been first proposed in [32], and due to its potential in enhancing the transmission reliability and the capacity of the system without penalizing the system resources, e.g. bandwidth and spreading codes, it has been subsequently adopted by the cdma2000 standard [33] [34].

Since its introduction, the STS scheme has been subjected to extensive performance analysis and evaluation (see [33] for example). Moreover, various studies have been conducted to compare the performance of the STS scheme with other open loop transmit diversity schemes, e.g. Space-Time Transmit Diversity (STTD) and the Orthogonal Transmit Diversity (OTD). A basic comparison between STS, STTD, and OTD has appeared in [35] for a CDMA system operating over flat fading channel with one user only and the channel was assumed to be perfectly known. In [36], the effect of the channel fading coefficients estimation errors on the performance of the uplink STS CDMA system has been investigated. It has been shown that as the number of multipath components increases, the estimation errors significantly impact

the system performance. In [37] and [38], the performance of a downlink STS-based CDMA system has been analyzed in frequency selective fading channel with imperfect estimation of the fading coefficients.

The majority of the relevant work in the literature suggests that the STS scheme is rather sensitive to the fading coefficients estimation errors especially when the channel is highly time dispersive. In realistic systems, however, channel estimation errors are composed of not only the errors in estimating the fading coefficients but also the errors in detecting the multipath components impinging at the receiver front end. The latter errors have profound effect on the performance of the system since estimating the fading coefficients of a certain multipath component is functionally carried out after that path is detected and identified. Hence, accurate multipath detection is of great interest for STS-based CDMA systems as it impacts the overall performance of the receiver. Up to date, neither the problem of multipath detection for STS-based CDMA systems nor the effect of imperfect multipath detection on the performance of STS scheme have been investigated.

The rest of this chapter is organized as follows. The signal model is described in Section 3.2. In Section 3.3, the EMDS and the IMDS are extended to work on the signal model under the STS scheme. Numerical results that compare the performance of both detection schemes are presented and discussed in Section 3.4. Finally, concluding remarks are given in Section 3.5.

3.2 Signal Model

The system considered here is similar to the proposed downlink cdma2000 system with space-time spreading. We assume that the base station transmitter is equipped with two antennas and the mobile terminal receiver utilizes one antenna, i.e., $(2, 1)$ STS scheme. The channel between the transmitter antennas and the receiver antenna is frequency selective Rayleigh fading channel. We assume BPSK modulation and spreading. Each transmitter antenna code-multiplexes a distinct pilot with the traffic signal.

The base station is assumed to serve M users. Each user is assigned two different codes from a set of orthogonal codes. A block diagram describing the spreading scheme is shown in Figure 3.1.

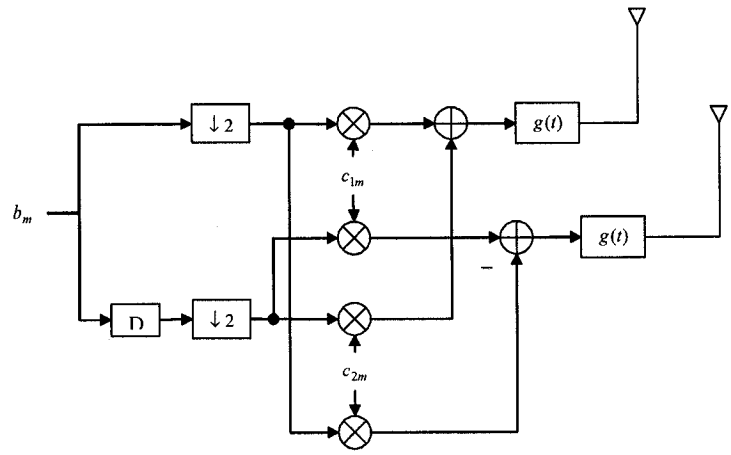

Figure 3.1: A $(2, 1)$ space-time spreading scheme.

After splitting the users' data into even and odd substreams, the transmitted traffic and pilot signals from the 1^{st} and 2^{nd} antennas, respectively, are modeled as

$$s_1(t) = \sum_{m=1}^{M} \left[\sqrt{\frac{E_{bm}}{2}} (a_{1m}(t) b_{1m}(n) + a_{2m}(t) b_{2m}(n)) \right] + \sqrt{\frac{G_p}{2}} a_{1(M+1)}(t) \tag{3.1}$$

$$s_2(t) = \sum_{m=1}^{M} \left[\sqrt{\frac{E_{bm}}{2}} (a_{1m}(t) b_{2m}(n) - a_{2m}(t) b_{1m}(n)) \right] + \sqrt{\frac{G_p}{2}} a_{2(M+1)}(t) \tag{3.2}$$

where, E_{bm} is the average bit energy for the m^{th} user, $b_{1m}(n) \in \{\pm 1\}$ is the n^{th} information bit in the even substream for the m^{th} user, similarly, $b_{2m}(n) \in \{\pm 1\}$ is the n^{th} information bit in the odd substream for the m^{th} user, G_p is the pilot channel power gain compared to the traffic channel, and $a_{q\lambda}(t)$ is the signature waveform

$$a_{q\lambda}(t) = \frac{1}{\sqrt{N_c}} \sum_{j=0}^{N_c-1} c_{q\lambda}(j) g(t - jT_c) \tag{3.3}$$

where, $\lambda \in \{1, 2, ..., M+1\}$, $q \in \{1, 2\}$, N_c is the spreading gain, $c_{q\lambda}$ is the spreading code assigned for the λ^{th} transmitted channel from the q^{th} antenna, $g(t)$ is the chip pulse shape, and T_c is the chip period. The spreading code used for a particular user or pilot channel is the multiplication of the channelization code assigned for that channel, e.g., Walsh code, with base station specific scrambling code.

The transmitted signal from each antenna traverses a multipath fading channel before it impinges at the desired user's receiver front end. The channel between each

transmitter antenna and the receiver antenna has L time varying paths. It is assumed that each pair of paths from both transmitter antennas arrives at the receiver with the same delay. This assumption is valid in practice since the propagation delays between the two transmit antennas are typically in the order of nanoseconds, while the multipath delays are measured in microseconds [33]. The channel between the two transmitter antennas and the receiver antenna is depicted schematically in Figure 3.2 where the l^{th} pair of paths, $\{\alpha_{1l}, \alpha_{2l}\}$ arrive at the receiver with delay τ_l.

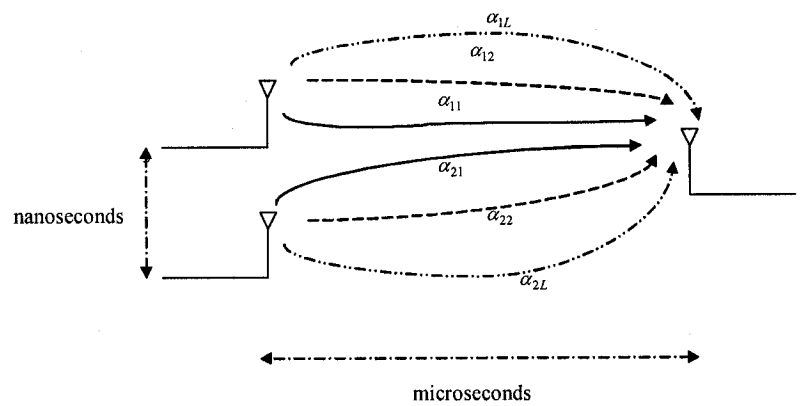

Figure 3.2: The channel structure between the transmitter antennas and the receiver antenna.

The total received signal at the m^{th} user's receiver is given by

$$r(t) = \sum_{l=1}^{L} [\alpha_{1l}(t)s_1(t-\tau_l) + \alpha_{2l}(t)s_2(t-\tau_l)] + w(t) \tag{3.4}$$

where $\alpha_{ql}(t)$ is the complex fading coefficient of the l^{th} path between the q^{th} antenna and the receiver antenna, τ_l is the delay of the l^{th} path pair, and $w(t)$ is complex additive white Gaussian noise (AWGN) with zero mean and power spectral density

$N_0/2$ per dimension. The channel coefficients $\{\alpha_{ql} : l = 1, 2, \ldots, L\}$ are modeled as independent and identically distributed (i.i.d.) complex Gaussian random variables with zero mean and variance $0.5\phi(\tau_l)$ per dimension, where $\phi(\tau)$ is the power delay profile (PDP), i.e., $|\alpha_{ql}|$ is Rayleigh distributed and the phase is uniformly distributed in $[0, 2\pi)$. The channel coefficients are assumed to be constant during a symbol duration, e.g. N_c chips.

After the multipath delays detection and channel estimation is performed, the received signal is processed by a RAKE receiver with L fingers as shown in Figure 3.3.

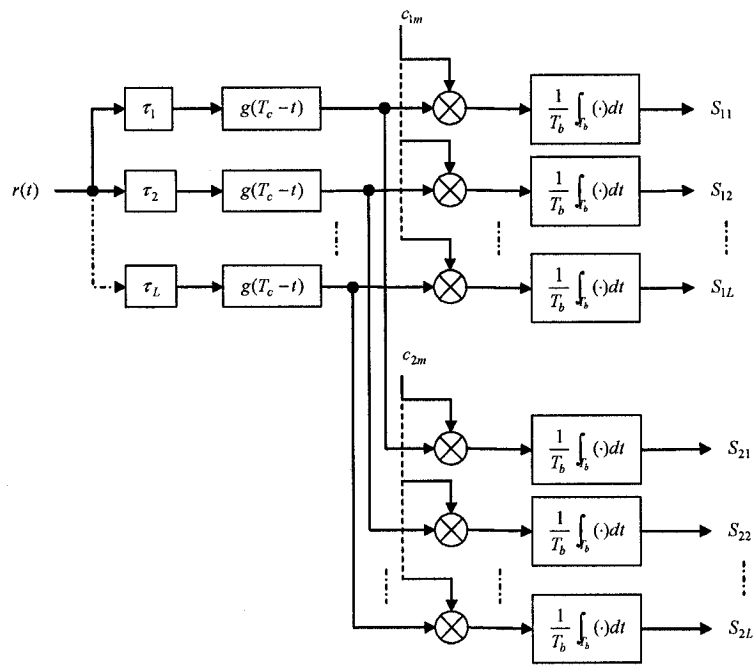

Figure 3.3: The RAKE receiver structure for $(2, 1)$ STS scheme.

The fingers are time aligned with the detected multipath components. After

alignment and chip match-filtering, each finger despreads the incoming signal using the 1^{st} and the 2^{nd} antennas' spreading codes. As seen in Figure 3.3, each of the despread signals obtained using the q^{th} antenna's code in the l^{th} finger, S_{ql}, is used by the STS decoder/combiner to recover the transmitted bits as follows.

$$\hat{b}_{1m} = sgn\left(\mathrm{Re}\left\{\sum_{l=1}^{L} \alpha_{1l}^{*}(n)S_{1l} - \alpha_{2l}^{*}(n)S_{2l}\right\}\right) \tag{3.5}$$

$$\hat{b}_{2m} = sgn\left(\mathrm{Re}\left\{\sum_{l=1}^{L} \alpha_{2l}^{*}(n)S_{1l} + \alpha_{1l}^{*}(n)S_{2l}\right\}\right) \tag{3.6}$$

where $sgn(x) = -1$ when $x < 0$ and 1 for $x \geq 0$, and $\alpha_{ql}^{*}(n)$ is the complex conjugate of the channel coefficient seen during the n^{th} bit duration in the l^{th} path between the q^{th} transmitter antenna an the receiver antenna.

In practice, the channel coefficients are estimated in each finger using a moving average filter over the pilot signal after proper alignment with the corresponding delay. Hence, if an incorrect path is detected and assigned to a RAKE finger, forged channel estimates will be obtained and used by the STS decoder. This essentially increases the transmission errors as it affects the demodulation of both data bits.

To investigate the impact of multipath detection on the bit-error rate (BER) performance of the STS scheme, the search algorithm and multipath detection for the system described above are in order.

3.3 The Search Algorithm and Multipath Detection

Designating the pilot channel transmitted from the q^{th} antenna as the j^{th} pilot channel, i.e. $j = 1, 2$, the search results obtained using the j^{th} pilot code are given by

$$h_{j,k}(n) = f_{jj,k}(n) + f_{j,Ik}(n) + f_{jq,lk}(n) + N_{kn}, \quad j \neq q \tag{3.7}$$

where the index k represents the k^{th} delay offset within the search window and n is the search time index within the received frame, $f_{jj,k}(n)$ is the contribution of the j^{th} pilot signal, $f_{j,In}(k)$ the interference coming from the traffic channels transmitted by both antennas, $f_{jq,lk}(n)$ is the interference seen due to the q^{th} pilot signal, and N_{kn} is the contribution of the AWGN noise. The condition $j \neq q$ simply means that the searcher attempts to despread the incoming signal using one pilot code at a time. The first component in (3.7) can be shown to be

$$f_{jj,k}(n) = \sqrt{\frac{G_p}{2}} \sum_{l=1}^{L} \alpha_{jl}(n) R_{j,j(M+1),kl} \tag{3.8}$$

where

$$R_{j,im,kl} = \frac{1}{\sqrt{T_b}} \int_{T_b} c_{jm} c_{im} g(t - \tau_l) g(t - \tau_k) dt, \; i = 1, 2 \tag{3.9}$$

The second and the third components in (3.7), can be found as

$$f_{j,In}(k) = \sum_{m=1}^{M} \sqrt{\frac{E_{bm}}{2}} \sum_{l=1}^{L} (\alpha_{1l}(n) [R_{j,1m,kl} d_{1m}(n) + R_{j,2m,kl} d_{2m}(n)] + \alpha_{2l}(n) [R_{j,1m,kl} d_{2m}(n) - R_{j,2m,kl} d_{1m}(n)]) \quad (3.10)$$

and

$$f_{jq,lk}(n) = \sqrt{\frac{G_p}{2}} \sum_{l=1}^{L} \alpha_{ql}(n) R_{j,q(M+1),kl} \quad (3.11)$$

The searcher should detect an effective path for the first user whenever l equals k, i.e., $\tau_l = \tau_k$, where the spreading waveform's autocorrelation function will be at its maximum. In this case, (3.8) can be written as

$$f_{jj,k}(n) = \sqrt{\frac{G_p}{2}} \alpha_{jk}(n) + \sqrt{\frac{G_p}{2}} \sum_{l \neq k}^{L} \alpha_{jl}(n) R_{j,j(M+1),kl}. \quad (3.12)$$

Now, the search result during the n^{th} time instant is written compactly as

$$h_{j,k}(n) = \sqrt{\frac{G_p}{2}} \alpha_{jk}(n) + I_{j,k}(n) \quad (3.13)$$

where

$$I_{j,k}(n) = \sqrt{\frac{G_p}{2}} \sum_{l \neq k}^{L} \alpha_{jl}(n) R_{jj,kl} + f_{j,In}(k) + N_{kn}.$$

To improve the probability of multipath detection, N_A independent search results are obtained through repeating the search process using each pilot at different time

instants, e.g. bits or search blocks, during a data frame. These time instants are usually chosen to be spaced sufficiently far from each other within a frame.

3.3.1 The EMDS

The conventional multipath detection scheme can be extended to cope with space time spreading scheme where two transmitter antennas are employed at the BS. As we have shown previously, two sets of independent search results are obtained by despreading the incoming signal with the pilot code for each antenna. For each set of results, the multipath detection metric is formulated as

$$Y_j(k) = \frac{1}{N_A} \sum_{n=1}^{N_A} |h_{j,k}(n)|^2. \tag{3.14}$$

Since each pair of paths between the transmitter antennas and the receiver antenna arrive at the receiver at after the same set of delays, the detection metrics resulting for both antennas can be averaged to yield the final detection metric as follows.

$$Y(k) = \frac{1}{2}[Y_1(k) + Y_2(k)]. \tag{3.15}$$

Averaging both detection metric will have the effect of increasing the probability of detecting the potential multipath components. The detection logic is similar to the one adopted for the conventional multipath detection scheme in Section 2.2.

3.3.2 The IMDS

As it has been shown in Section 2.4, an improved multipath detection scheme can be developed based on estimating the interference power seen at each delay offset and subtracting this power from the total received power at that delay. To estimate the interference power, coarse channel estimates at the search instants are used. The channel estimates of the paths from the j^{th} transmitter antenna to the receiver antenna at the k^{th} delay offset $\hat{h}_{jk}(n)$ are obtained by filtering the search results using an FIR filter $f(n)$ as follows

$$\hat{h}_{j,k}(n) = \sum_{m=0}^{K_f-1} f(m)h_{j,k}(m-n). \tag{3.16}$$

Having the channel estimates, the interference variance seen in the paths from the j^{th} transmitter antenna to the receiver antenna at the k^{th} delay offset $\hat{\sigma}^2_{j,I}(k)$ is estimated using the following estimator.

$$\hat{\sigma}^2_{j,I}(k) = \frac{1}{N_A}\sum_{n=1}^{N_A} |h_{j,k}(n) - \hat{h}_{j,k}(n)|^2. \tag{3.17}$$

For the search results obtained from the pilot channel transmitted from the j^{th} antenna , the detection metric of the improved multipath detection scheme is formulated by subtracting the estimated interference variance from the total power at each

delay in the search window. Hence, the detection metric becomes

$$Z_j(k) = Y_j(k) - \hat{\sigma}^2_{j,I}(k). \tag{3.18}$$

Similar to the conventional multipath detection scheme, the detection metrics obtained from the search results using both pilots can be averaged as

$$Z(k) = \frac{1}{2}[Z_2(k) + Z_1(k)]. \tag{3.19}$$

3.4 Simulation Results

A forward link CDMA system with a $(2, 1)$ space-time spreading scheme has been considered for simulation. The relevant system parameters are listed below.

- Number of users in the sector $M = 20$ (with equal power).
- The spreading factor: 128
- Number of paths $L = 3$, with relative delays $[0, 4, 8]$ chips and uniform power delay profile, i.e. $\phi(\tau_l) = 1/L \ \forall l$.
- Number of accumulated search results per pilot $N_A = 12$.
- Normalized Doppler rate: 10^{-3}.

- The length of the FIR filter $K_f = 6$ (rectangular window)
- Pilot power Gain: $Gp = 10$, 15, 20 % of the total power transmitted from the BS, i.e. 3.5, 5.5, and 7 dB relative to a single traffic channel.
- The fading coefficients are estimated for the assigned RAKE fingers using a moving average filter of length 12 operating over the pilot symbols.

Figure 3.4 shows the receiver operational characteristics (ROC) for both detection schemes. The probability of detecting the first path is plotted against the probability of false alarm at $E_b/N_0 = 8$ dB for different pilot power gains. It is evident that the IMDS enhances the receiver operational characteristics considerably compared to the EMDS. At the same pilot power gain, e.g. $Gp = 7$ dB, the IMDS results in higher probability of detection at any given practical probability of false alarm. For instance, at probability of false alarm of 1%, while the EMDS results in probability of detection of around 77% , the IMDS results in probability of detection of around 95%. This means that the IMDS misses the first path only 5 percent of times while EMDS misses that path 23 percent of the times when both schemes allow false alarms to occur at a rate of 1%. It is also interesting to observe that the IMDS with pilot power gain of 3.5 dB outperforms the EMDS operating at pilot power gain of 7 dB. As far as multipath acquisition is concerned, this result implies that the IMDS with $Gp = 3.5$ dB is, at least, equivalent to the EMDS with $Gp = 7$ dB.

The probability of accurately assigning the first path to a RAKE finger as a function of E_b/N_0 is investigated using Figure 3.5 where the probability of false alarm

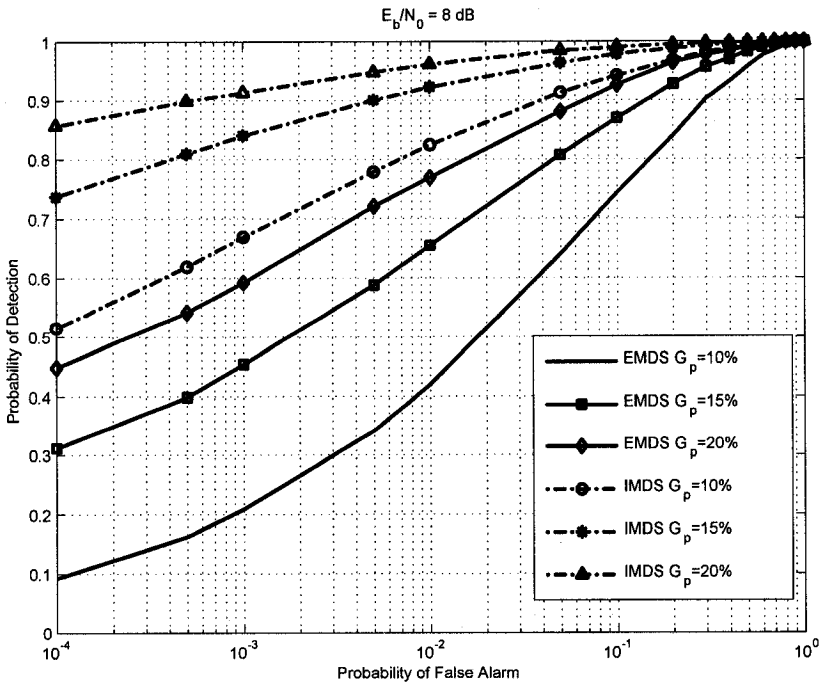

Figure 3.4: The ROC produced by the EMDS and IMDS at $E_b/N_0 = 8$ dB for different pilot power gains.

is set to 1%. As shown in the figure, the IMDS is more capable of identifying the first path and assigning it to one of the RAKE fingers than the EMDS. Once again, the efficiency of the IMDS in utilizing the pilot power is illustrated by comparing the IMDS with $Gp = 3.5$ dB to the EMDS with $Gp = 7$ dB.

For diversity combining, the ability of the assignment scheme to allocate all the potential paths to the RAKE fingers impacts the receiver performance. In Figure 3.6, the probability of accurately assigning all the three paths to the available RAKE fingers for both detection schemes is depicted as a function of E_b/N_0 for different pilot power gains. It is clear that the IMDS maintains a superior assignment performance compared to the EMDS.

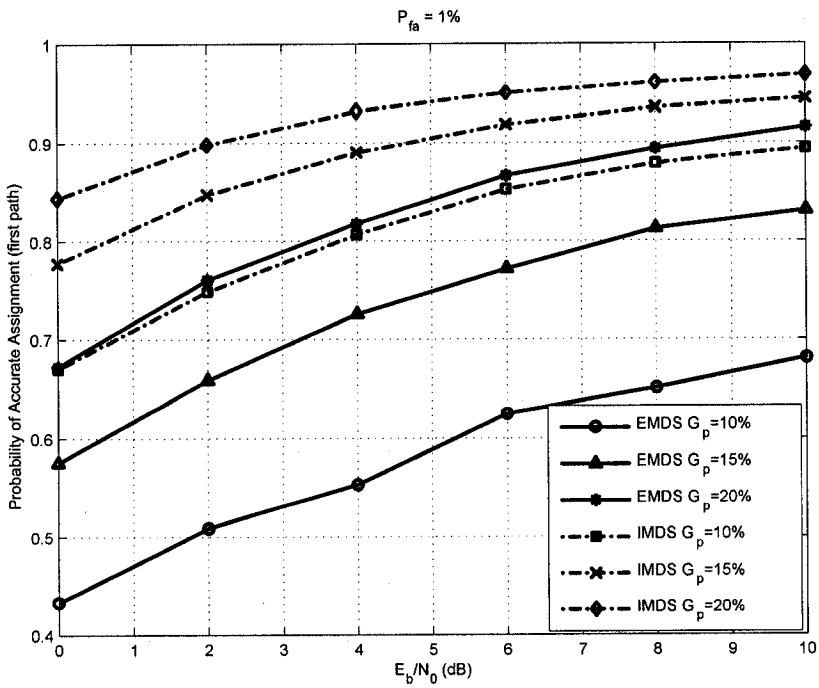

Figure 3.5: The probability of accurate assignment of the first path as a function of E_b/N_0 at different pilot power gains for both schemes.

Figure 3.7 shows the BER performance of the receiver as a function of E_b/N_0 for different pilot power gains. The ideal performance (when the channel is perfectly known) is also shown in the same finger. It is evident that the deficiency of the EMDS in detecting the potential paths significantly deteriorates the BER performance. As the pilot power increases the gap between the ideal and practical performance is reduced since better estimates of the delays and the fading coefficients are used for combining. For the EMDS, the performance gap is almost 3.5 dB with $G_p = 20\%$ at high E_b/N_0. Utilizing the IMDS with the same pilot power, however, results in reducing the gap to almost 1.5 dB indicating that the IMDS provides a gain of around 2 dB compared to the EMDS at high E_b/N_0. We observe also that IMDS with

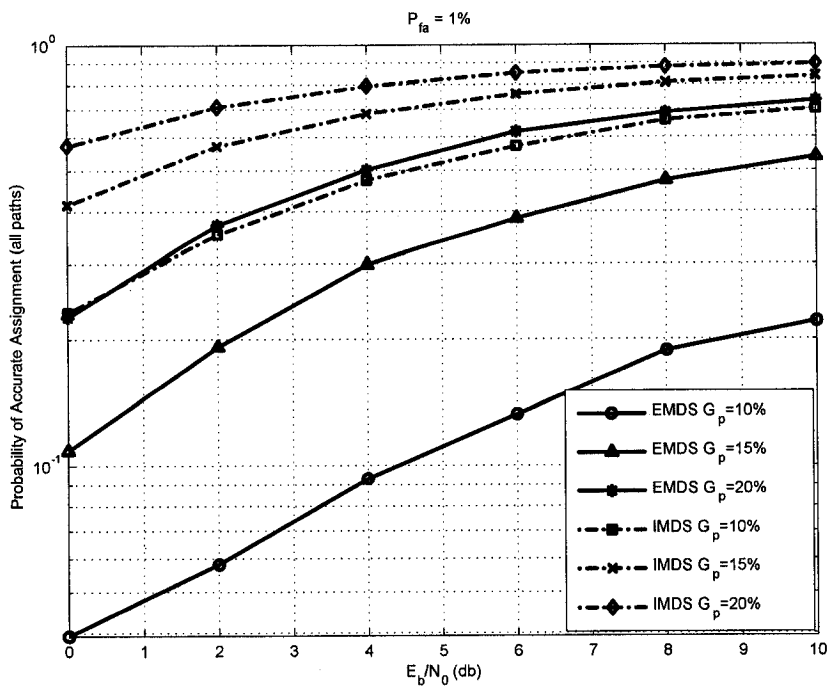

Figure 3.6: The probability of accurate assignment of the three paths as a function of E_b/N_0 at different pilot power gains for both schemes.

$G_p = 10\%$ draws the same BER performance as that of the EMDS with $G_p = 20\%$ suggesting that the IMDS saves at least 3.5 dB of the pilot power.

The obtained BER results are consistent with detection and assignment results shown in Figures 3.4, 3.5, and 3.6. The IMDS provides the RAKE with the accurate path delays most of the times even when the pilot power is low. Consequently, the channel is estimated for the correct paths. The EMDS, on the other hand, results in assigning wrong path delays to the RAKE fingers, which in turn, increases the channel estimation errors drastically.

As it has been demonstrated in [36], there is practical trade-off between the diversity order and the pilot power. Meaning that, the number of transmitter antennas is

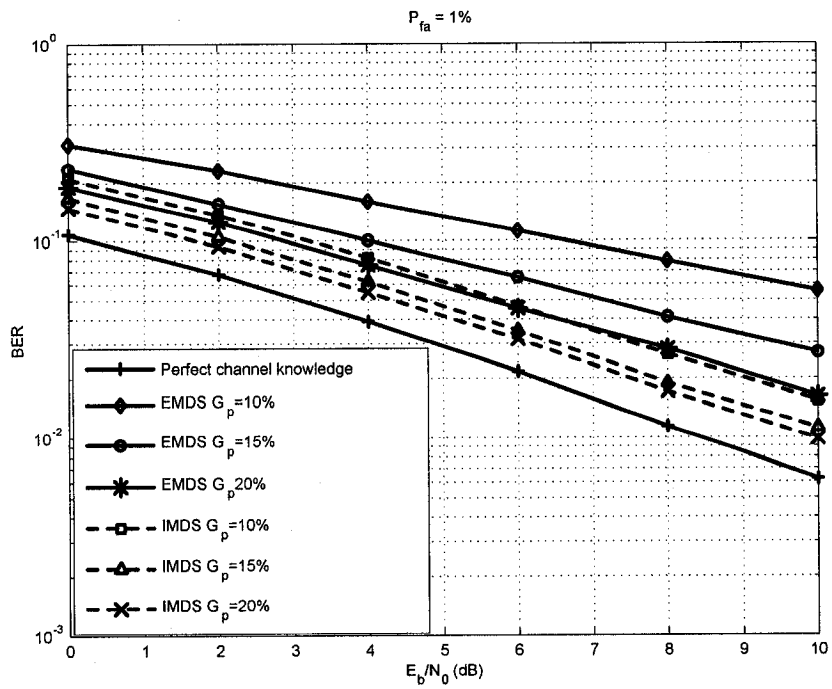

Figure 3.7: The BER performance of the $(2,1)$ STS scheme as a function of E_b/N_0 and the pilot power as parameter when the paths are perfectly known, and when they are detected and assigned based on the EMDS and IMDS.

typically limited by the available pilot power. This trade-off is brought about by the channel estimation errors which increase as a pilot power decreases. Consequently, the potential of the IMDS in reducing the required pilot power compared to the EMDS is particularly appealing to the implementation of the STS schemes.

3.5 Conclusions

In this chapter, we have investigated the impact of imperfect multipath detection on the performance of CDMA systems employing space-time spreading (STS). The conventional (EMDS) and the improved (IMDS) multipath detection schemes have

been extended to work on the signal model assumed by the STS scheme.

It has been shown that imperfect multipath detection as provided by the EMDS deteriorates the system performance substantially. The IMDS, however, has resulted in closing the performance gap between the ideal and realistic systems considerably. Furthermore, the IMDS has shown great promise in reducing the required pilot channel power.

Chapter 4

Conclusions and Future Work

Nowadays, the wireless communication systems are ought to support very high data rates for a maximum number of subscribers. To this end, the third generation (3G) wireless mobile communication systems are being standardized around the world. As a matter of fact, some of the existing 3G standards are already deployed in some countries.

In this work, the multipath detection problem and finger assignment algorithms for CDMA systems have been addressed and investigated thoroughly. The conventional energy based multipath detection scheme (EMDS) has been analyzed. Based on remedying the main deficiency of the conventional scheme, an improved multipath detection scheme (IMDS) has been proposed and analyzed. Relative to the EMDS, the performance improvement of the IMDS has been examined in various communication environments not only for the conventional CDMA systems, but also for the recently proposed CDMA systems with space-time spreading.

4.1 Concluding Remarks

Conventionally, multipath detection and finger assignment have been based on the energy content per multipath component. To measure the aggregate energy each path carries, a search algorithm is applied using the pilot channel and the used pseudo-random code. Nevertheless, the conventional multipath detection scheme (EMDS), suffers from many drawbacks.

Among all, the basic drawback of the EMDS is brought about by its ignorance of the interference contaminating the received signal per path, and hence, it results in low probability of detection at low SINR. The proposed IMDS, on the other hand, has been developed such that its multipath detection metric is more immune against noise and interference as compared to the EMDS. This has been accomplished by estimating the aggregate interference power seen at each path, and thereupon, subtracting this estimate from the total energy content of that path. To estimate the interference variance at each delay offset, a simple estimation circuitry has been designed and incorporated into the CDMA receiver structure with a rather moderate additional complexity.

The analytical and simulations results have demonstrated the promising improvement provided by the IMDS over the EMDS in terms of many performance measures. In terms of the detection performance, the IMDS has the effect of increasing the probability of detection and decreasing the probability of false alarm as compared to the EMDS. Consequently, the IMDS has the potential of expanding the operational

region of the CDMA receiver by reducing the influence of the noise and interference on the detection process. It has been shown that the IMDS has the effect of reducing the power consumption of the mobile terminal considerably by efficiently utilizing the pilot power. This is particularly appealing since the mobile terminal typically has limited power resources.

In terms of the bit-error-rate performance of the RAKE receiver, the IMDS has shown significant improvement as compared to the EMDS. This is justifiable by the superior finger assignment performance drawn by the IMDS. As opposed to the EMDS, the IMDS has the capability of assigning the correct multipath delays to the RAKE fingers with a higher probability under various operation conditions.

For multipath detection and finger assignment purposes in the recently proposed CDMA systems with space time spreading, both the EMDS and IMDS have been extended to cope with the spatial dimension of the channel. The effect of imperfect multipath detection on the performance of the STS scheme has been investigated. It has been shown that imperfect multipath detection as drawn by the EMDS deteriorates the system performance substantially. The IMDS, however, has resulted in reducing the performance gap between the ideal and realistic systems considerably. It has been also shown that the IMDS maintains the same improvement aspects encountered in the conventional CDMA systems. The IMDS has shown, once again, a superior finger assignment performance, which in turn, has resulted in a significant BER performance gain compared to the EMDS. Remarkably, the EMDS has shown great efficiency in utilizing the pilot power transmitted from the base station.

During this work, a special attention has been paid to realize practical solutions for the multipath detection and finger assignment problems in CDMA systems. Consequently, the proposed detection and assignment schemes have been implemented with the lowest possible complexity. Hence, and with an eye on the performance of these schemes compared to the conventional ones, the proposed solutions constitute prominent candidates for deployments.

4.2 Future Work

In this work, it has been remarked that there is still a considerable performance gap between the ideal receiver performance, i.e. when the delays are known, and the performance drawn by the EMDS and IMDS. This basically suggests that there is definitely room for future work on the area of multipath detection and finger assignment. Some of the research issues to be considered in the future are highlighted in the following.

- Better channel estimates would boost the performance of the IMDS, and consequently, closing the performance gap between the ideal and practical systems. Thus, future work may involve improving the channel coefficients estimation at the acquisition stage.

- As it has been observed, the IMDS is much more efficient in utilizing the pilot power as compared to the EMDS. An investigation of interest is to study the maximum allowable number of antennas utilized for the space-time spreading

schemes when the IMDS and EMDS are deployed with limited pilot power. It is expected that, for the same pilot power, the IMDS will allow for doubling the number of antennas as compared to the EMDS, i.e. increasing the diversity order, and consequently, enhancing system performance.

- Although the adaptive acquisition problem has not been addressed herein, implementing the IMDS as an adaptive acquisition scheme seems promising and shall be considered in the near future.

Bibliography

[1] S. Lee and J. Kim, "Performance analysis of DS-SS PN code acquisition systems using soft-decision techniques in a Rayleigh-fading channel," *IEEE Trans. on Vehicular Tech.*, vol. 51, no. 6, pp. 1587-595, Nov. 2002.

[2] D. Banerjee. and A. Paulraj, "Location-aided RAKE receiver finger assignment," *Proc., IEEE Global Telecommunications Conference (GLOBCOM)*, pp. 1043-1047, 2003.

[3] J. Delva. and I. Howitt, "PN acquisition for DS/SS using a preloop parallel binary search phase estimator and a closed-loop selective search subsystem," *IEEE Trans. on Wireless Commun.*, vol. 3, no. 2, pp. 408 -417, March 2004.

[4] E. Sourour, and S. Gupta, "Direct-sequence spread spectrum parallel acquisition in fading mobile channel," *IEEE Trans. on Comm.*, vol 38, no. 7, pp. 992-998, July 1990.

[5] L. Milstein., J. Gevargiz and P. Das, "Rapid acquisition for direct sequence spread-spectrum communications using parallel SAW convolvers," *IEEE Trans. on Commun.*, vol com-33, no. 7, pp. 593-600, July 1985.

[6] K. Cheun, "Performance of direct-sequence spread-spectrum RAKE receivers with random spreading sequences," *IEEE Trans. Commun.*, vol. 45, no. 9, pp. 1130-1143, Sept. 1997.

[7] B. Vijlgaard, P. Mongensen and J. Knudsen, "Grouped rake finger management principle for wideband CDMA," *Proc. IEEE VTC*, pp. 87-91, 2000.

[8] K. Balashandran, K. Chang and K Rege, "Rake receiver finger assignment in CDMA terminals with fractionally spaced multipaths," *Proc. IEEE VTC*, pp. 476-481, 1999.

[9] K. Chang-Joo, H-J. Lee and H-S. Lee, "Adaptive acquisition of PN sequences for DSSS communications," *IEEE Trans. on Commun.*, vol. 46, no. 8, pp. 993-996, August 1998.

[10] A. Rehan, A. Chaturvedi, "New adaptive serial search PN code acquisition scheme for DS-CDMA systems," *Proc. IEEE ICPWC*, pp. 245-248, 2000.

[11] K. Chang-Joo, "Adaptive acquisition of PN code in multipath fading channels," *IEE Electronics Letters*, vol. 38, no. 2, pp. 135-137, Jan. 2002.

[12] K. Chang-Joo, "Acquisition of PN code with adaptive threshold for DS/SS communications," *IEE Electronics Letters*, vol. 33, no. 16, pp. 135-137, July 1997.

[13] H. Park and B. Kang, "On serial search code acquisition for direct sequence spread spectrum system: Application to IS-95 CDMA system," *Proc. IEEE VTC*, pp. 291-295, July 1995.

[14] S. Chung, "New serial search acquisition approach with automatic decision threshold control," *Proc. IEEE VTC*, pp. 530-536, July 1995.

[15] R. Zhang, Y. Li, T. Tjhung, and H. Zhang., "RAKE reception with improved maximal ratio combining weights for the WCDMA forward link," *Proc. IEEE 3G Wireless Conference*, pp. 763–768, 2001.

[16] D. L. Noneaker, "Optimal Combining for Rake Reception in Mobile Cellular CDMA Forward Links," *Proc. IEEE Militiary Commun. Conf.*, pp. 842–846,, 1998.

[17] W. Jakes, Y. Yeh, M. Gans, and D. Reudink, *Microwave Mobile Communications*, IEEE Press, 1974.

[18] M. Abou-Khousa , M. El-Tarhuni , and A. Ghrayeb , "A Novel Finger Assignment Algorithm for RAKE Receivers in CDMA Systems," *Proc. IEEE Intern. conf. on commun.* ICC-04, pp. 2516-2520, June 2004.

[19] M. Abou-Khousa, A. Ghrayeb, and M. El-Tarhuni, "Signal-to-interference ratio estimation in CDMA systems," *Proc. of IEEE Canadian Conference on Electrical and Computer Engineering*, CCECE 2004, pp. 1333-1337, May 2004.

[20] M. Abou-Khousa, M. El-Tarhuni, "SIR-based RAKE receiver finger assignment algorithm," *Proc. of 10th IEEE intern. conf. on electronics, circuits and systems*, ICECS 2003, pp. 639-642, Dec. 2003.

[21] G. L. Stüber, Principles of Mobile Communication, 2^{nd}Edition, Kluwer Academic Publishers, 2001.

[22] A. Viterbi, Principles of Spread Spectrum Communications, Addison Wesley Longman, Inc., USA, 1995.

[23] J. Lehnert, and M. Pursley, "Error probabilities for binary direct-sequence spread-spectrum communications with random signature sequences," *IEEE Trans. Commun.*, vol. com-35, no. 1, pp. 87-98, Jan. 1987.

[24] J. Holtzman, "A simple, accurate method to calculate spread spectrum multiple-access error probabilities," *IEEE Trans. Commun.*, vol. 40, no. 3, pp. 461-464, March 1992.

[25] E. Ström, and F. Halmsten, "A maximum likelihood approach for estimating DS-CDMA multipath fading channels," *IEEE Journal on Selec. Areas of Commun.*, vol. 18, no. 1, pp. 132-140, Jan. 2000.

[26] L. Peterson, E. Ziemer, E. Borth, *Introduction to Spread Spectrum Communications*, NJ, Prentice Hall, 1995.

[27] J. G. Proakis, *Digital Communications*, 4^{th} Edition, New York: McGraw-Hill, 2000.

[28] S. Kay, Fundamentals of Statistical Signal Processing; Estimation Theory, Prentice Hall, Vol. 1, 1993.

[29] R. Schmidt, "Multiple emitter location and signal parameter estimation," *IEEE trans. on antenna and propag.*, vol AP-34m no. 3, pp. 276-280, March 1986.

[30] H. Boujemaa and M. Siala, "On a maximum likelihood delay axquisition algorithm," *Proc. IEEE Intern. conf. on commun.* ICC-01, pp. 2510-2514, June 2001.

[31] Q. Zhang; J. Huang, and Y. Xie, "High resolution delay estimation," *Proc. 1993 IEEE Region 10 Conf. on Computer, Commun., Control and Power Eng.*, TENCON'93, pp. 579-583, 19-21 Oct. 1993.

[32] C. Papadias, B. Hockwald, T. Marzetta, M. Buehrer, and R. Soni, "Space-time spreading for CDMA systems," *Proc.* 6^{th} *workshop smart antennas wireless mobile commun.*, Stanford, CA, July 22-23, 1999.

[33] B. Hockwald, T. Marzetta, and C. Papadias, "A transmitter diversity scheme for wideband CDMA systems based on space-time spreading," IEEE Jour. selec. areas in commun., vol 19, no. 1, pp. 48-60, Jan., 2001.

[34] 3GPP2, C.S0002-A, *Physical layer standard for cdma2000 spread spectrum systems*, publication version, June, 2000.

[35] Y. Qiang and D. Li, "Performance analysis of several open-loop transmit diversity schemes for IMT-2000 systems," *Proc. intern. conf. on commun tech.*, ICCT 2003, pp. 1107-1110, 9-11 April 2003.

[36] L. L, Chong and L.B. Milstein, "The performance of a space-time spreading CDMA system with channel estimation errors," *Proc. IEEE intern conf. commun.*, ICC 2002, pp. 1793-1797, 28 April-2 May 2002.

[37] G. Wu, H. Wang; M. Chen; and S. Cheng, "Performance comparison of space-time spreading and space-time transmit diversity in cdma2000," *Proc. IEEE Vehicular Technology Conference,* VTC 2001 Fall, pp. 442-446, 2001.

[38] G. Wu, H. Wang; M. Chen, S. Cheng, and J. Lilleberg, "Performance Evaluation of Space Time spreading and orthogonal transmit diversity in cdma2000," *IEEE* 7^{th} *int. symp. spread-spectrum & appl.*, Pargue, Czech Republic, Sept., 2-5, 2002.